

An overview and recent advances in electrocatalysts for direct seawater splitting

Hao-Yu Wang, Chen-Chen Weng, Jin-Tao Ren, Zhong-Yong Yuan (✉)

Key Laboratory of Advanced Energy Materials Chemistry (Ministry of Education), School of Materials Science and Engineering, Nankai University, Tianjin 300350, China

© Higher Education Press 2021

Abstract In comparison to pure water, seawater is widely accepted as an unlimited resource. The direct seawater splitting is economical and eco-friendly, but the key challenges in seawater, especially the chlorine-related competing reactions at the anode, seriously hamper its practical application. The development of earth-abundant electrocatalysts toward direct seawater splitting has emerged as a promising strategy. Highly efficient electrocatalysts with improved selectivity and stability are of significance in preventing the interference of side reactions and resisting various impurities. This review first discusses the macroscopic understanding of direct seawater electrolysis and then focuses on the strategies for rational design of electrocatalysts toward direct seawater splitting. The perspectives of improved electrocatalysts to solve emerging challenges and further development of direct seawater splitting are also provided.

Keywords seawater splitting, electrocatalysts, oxygen evolution reaction, hydrogen evolution reaction, chlorine chemistry

1 Introduction

Renewable energy technologies are urgently needed in the face of severe environmental pollution and energy crises and limited supplies of fossil fuels [1–3]. Hydrogen, a promising energy carrier possessing high gravimetric energy density and environmental friendly features, can be obtained via water electrolysis technology from renewable energy such as sunlight or wind and further converted to other fuels or directly used in hydrogen fuel cells [4–6]. Typically, overall water electrolysis involves

two key reactions, including oxygen evolution reaction (OER) and hydrogen evolution reaction (HER), both of which require efficient electrocatalysts to accelerate the sluggish kinetics for high energy efficiency [7–10]. Recent years, many achievements have been made in developing non-precious OER/HER electrocatalysts as alternatives for Pt/C and Ir/Ru based catalysts [11–13]. However, biomass gasification and fossil fuels bear the main responsibility for hydrogen production with only 4% left to the electrochemical water splitting in the current case [14,15].

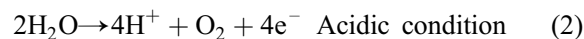
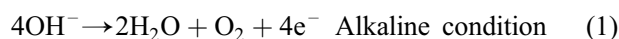
Low system efficiency of 70% and high cost result in the circumscribed application of water electrolysis since high purity water feeds are indispensable in commercially available water electrolyzers [16–18]. Actually, freshwater has been a scarce resource in many areas, especially in hot arid regions. The construction of an electrolytic water system must include water purification/desalination equipment for purification/desalination pre-treatment of saline and low-grade water [19,20]. Practical electrolyzers differ greatly from simple laboratory systems in which they involve complex configurations such as controlling the flow of input-fluid and outflow-air streams, gas regulators and thermal management devices. While the introduction of additional water purification systems inevitably entails prohibitive costs, even without taking into account related investments in transport and maintenance. Based on the consideration of cost reduction, direct use of saline seawater in water electrolysis system can be a promising and operational approach for coastal arid zones and offshore large-scale hydrogen productions. Removal of pre-treatment systems for purification/desalination can greatly improve economic efficiency.

The key step for the implementation of direct seawater electrolysis is developing suitable electrode catalysts with selective and stable electrocatalytic performance in seawater. However, it is known that seawater is a complex solution with high content of different salts up to 3.5%, in which various competing redox reactions and dramatic pH

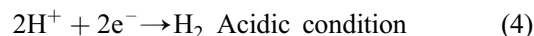
fluctuations result in the degradation and biofouling of catalysts [21]. Thus, in this review, a macroscopic understanding of direct seawater electrolysis is first discussed, and the difference between electrolysis in pure water and seawater is revealed. Then, we will focus on effective strategies for the rational construction of electrocatalysts with improved selectivity and stability on both electrodes based on the possible electrochemistry involved in this process. Recent achievements will be discussed for the guidelines of future research.

2 Overview of direct seawater electrolysis

Seawater splitting into hydrogen and oxygen is fundamentally identical to that in pure water, in which external electric energy is required to drive OER at the anode and HER at the cathode, and is eventually stored in the chemical bond between oxygen and hydrogen. The anode OER is a four-electron transferring reaction with several intermediates involving, which can be described by Eqs. (1) or (2) in alkaline or acidic conditions, respectively.



On the counter side of cathode, the two-electron transferring HER is the main reaction, which can be described by Eqs. (3) or (4) in alkaline or acidic environments, respectively.



However, unlike pure water, the composition of seawater is quite complex and varies from region to region [22,23]. In the average state, the overall salt concentrations of all ions are measured to be 3.5 wt-% and there are 11 ions with a concentration of more than $0.0005 \text{ mol} \cdot \text{kg}_{\text{H}_2\text{O}}^{-1}$, including Cl^- of $0.5658 \text{ mol} \cdot \text{kg}_{\text{H}_2\text{O}}^{-1}$, SO_4^{2-} of $0.0293 \text{ mol} \cdot \text{kg}_{\text{H}_2\text{O}}^{-1}$, Br^- of $0.0009 \text{ mol} \cdot \text{kg}_{\text{H}_2\text{O}}^{-1}$, Na^+ of $0.4862 \text{ mol} \cdot \text{kg}_{\text{H}_2\text{O}}^{-1}$, Mg^{2+} of $0.0548 \text{ mol} \cdot \text{kg}_{\text{H}_2\text{O}}^{-1}$, Ca^{2+} of

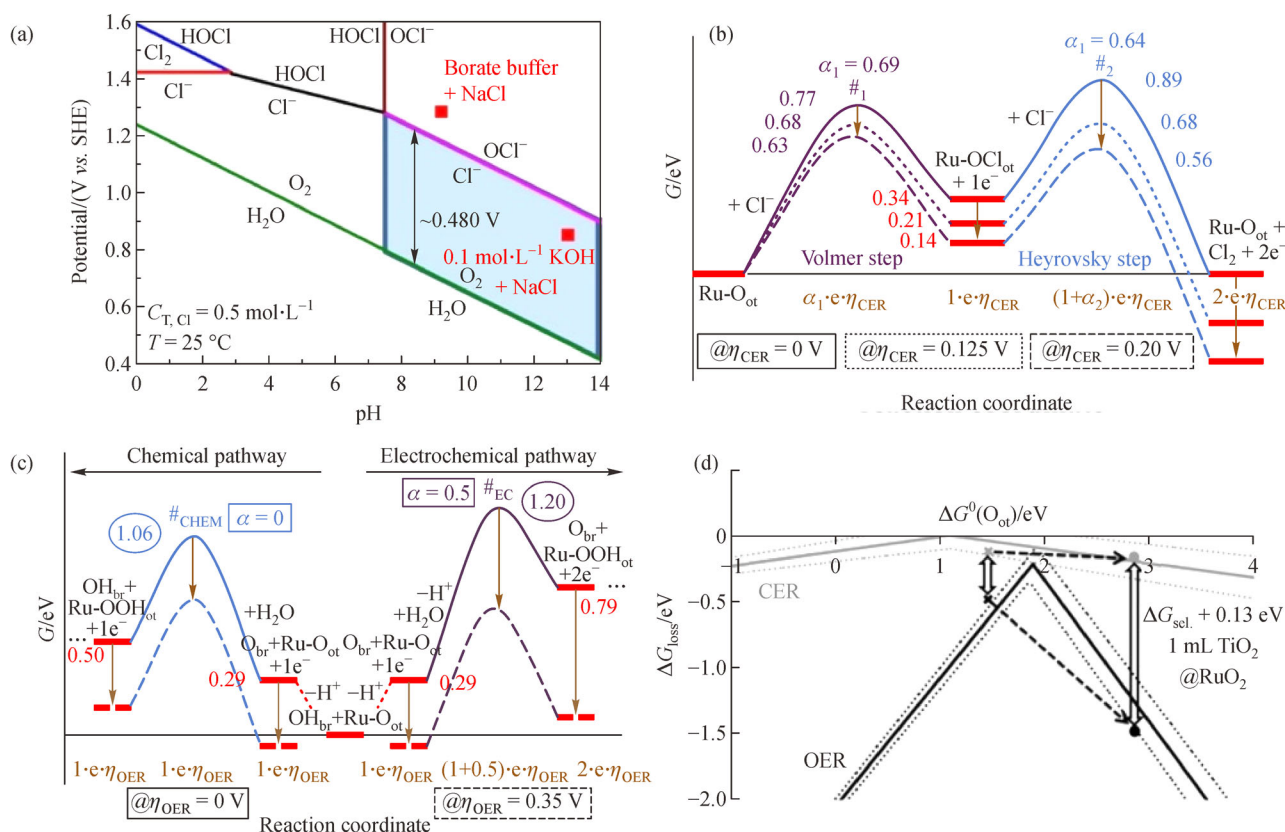


Fig. 1 Illustrations for the mechanisms of OER vs. chloride chemistry. (a) The Pourbaix diagram of an artificial model solution ($0.5 \text{ mol} \cdot \text{L}^{-1} \text{ NaCl}$ solution with electrolytes to control the pH and no other chlorine species) depicting the thermodynamic equilibrium of $\text{H}_2\text{O}/\text{O}_2$ (green line) and $\text{Cl}^-/\text{Cl}_2\text{-HOCl-OCl}^-$ (red line). Reprinted with permission from ref. [24], copyright 2016, Wiley-VCH. Free energy diagram over $\text{RuO}_2(110)$ for (b) CIER Volmer-Heyrovsky mechanism and (c) two OER competing water splitting reactions (electrochemical and chemical pathway) at different potentials. Reprinted with permission from ref. [25], copyright 2018, American Chemical Society. (d) ΔG_{loss} volcano diagram for OER (black) and chloride evolution reaction (CIER, gray). Reprinted with permission from ref. [26], copyright 2014, Wiley-VCH.

0.0105 mol·kg_{H₂O}⁻¹, K⁺ of 0.0106 mol·kg_{H₂O}⁻¹, B(OH)₃ of 0.0003 mol·kg_{H₂O}⁻¹, B(OH)₄⁻ of 0.0001 mol·kg_{H₂O}⁻¹, HCO₃⁻ of 0.0018 mol·kg_{H₂O}⁻¹ and CO₃⁻ of 0.0003 mol·kg_{H₂O}⁻¹. Based on the composition of seawater, the challenges of direct seawater electrolysis can be inferred in order to find solutions.

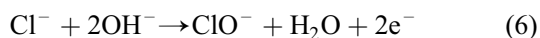
More than 0.5 mol·kg_{H₂O}⁻¹ Cl⁻ exists in seawater, leading to complicated chloride chemistry in direct seawater electrolysis and the specific competing reaction in the practical reaction condition under the influence of temperature, pH values and the most-important applied potentials. For simplicity, Dionigi et al. [24] considered the total concentration of Cl⁻ and other chlorine species as 0.5 mol·L⁻¹ and constructed a Pourbaix diagram (Fig. 1) to illustrate the chloride chemistry in seawater electrolysis, as shown in Fig. 1(a).

In acidic environments, the dominant competing reaction of chloride chemistry is CIER, formulated by Eq. (5).



The CIER does compete with OER in acid conditions even though it is thermodynamically unfavorable compared with OER according to the Pourbaix diagram, which is due to the kinetic superiority of CIER. This means that OER usually has a higher potential, making CIER the dominant reaction at the anode of seawater electrolysis for many catalysts.

In contrast, the Pourbaix diagram shows that the hypochlorite formation reaction gradually establishes its dominant position along with the increased pH and becomes unshakable in alkaline conditions when pH is higher than 7.5, formulated by Eq. (6).



Similarly, hypochlorite formation reaction is also a two-electron reaction with kinetic advantage over OER. Nevertheless, unlike CIER in acidic environment, hypochlorite formation reaction is very disadvantageous in comparison with OER in alkaline conditions, whose standard electrode potential follows the change of that of OER with a fixed difference of about 0.48 V. This means a maximum overpotential of 0.48 V for the OER electrocatalysts in alkaline conditions without any interference of any chlorine chemistry. Though OER and CIER also have differences in standard electrode potential in acid media, the allowed overpotential region where CIER is thermodynamically prohibited is much smaller and cannot support a relatively high current in direct seawater electrolysis. Associated with the fact that many non-precious electrocatalysts suffer degradation in acidic environment, alkaline environment seems to be more suitable for seawater splitting. Based on the above considerations, Strasser et al. [24] established an “alkaline design criterion” for non-noble metal-based electrocatalysts for selective anode

OER in seawater as Eq. (7).

$$\eta_{\text{OER}} \leq 480 \text{ mV at pH} > 7.5 \quad (7)$$

Further comprehension of the competition between OER and CIER at the anode of seawater electrolysis is of great significance to develop efficient OER electrocatalysts with high selectivity. Single crystalline RuO₂ (110) was chosen to be the model catalyst for studies in identifying reaction intermediates (RI), transition states (TS) and free energies of OER and CIER in acidic seawater by Over and coworkers [25]. For CIER, Volmer-Heyrovsky mechanism is the most accepted among the existing three mechanisms, involving the discharge and adsorption of Cl⁻ on Ru-O_{ct} combined by uncoordinated Ru sites and on-top oxygen (O_{ct}) to form the Ru-O_{ct}Cl RI (Volmer step) and the combination of a free Cl⁻ and an adsorbed Cl to form released Cl₂ (Heyrovsky step). As described in the free energy diagram of CIER at different overpotentials (Fig. 1 (b)), only one intermediate is involved, where Heyrovsky step is the rate determining step because of its high TS free energy. Besides, the TS free energy obviously decreases at the potentials of 0.125 and 0.20 V, making the CIER more kinetically favorable. Unlike CIER, the kinetically slower OER on RuO₂ (110) with complete O-capped surface involves several intermediates. Figure 1(c) shows the OER free energy diagram and describes two competing pathways, including chemical pathway and electrochemical pathway of the RI. The diagram illustrates that the electrochemical pathway becomes favorable over the chemical pathway when overpotential is larger than 0.3 V. Furthermore, the competition between CIER and OER was evaluated by using unfavorable Gibbs free energy (ΔG_{loss}) as the identifier of activity [26]. Figure 1(d) shows a ΔG_{loss} volcano diagram for CIER and OER. It is obvious that both CIER and OER obtain maximum activity at the middle value of $\Delta G^0(\text{O}_{\text{ct}})$ and the slope of OER is increased as the incorporation of three RI. The selectivity for OER is expressed by the difference in ΔG_{loss} values, which can be manipulated by several methods, i.e., the RuO₂ (110) with TiO₂ monolayer.

The high-concentration Cl⁻ not only lead to competing chlorine chemistry, but also bring out the corrosion of electrodes. Seawater is an extremely hostile environment due to the high corrosion capacity of Cl⁻. Corrosion studies (electrochemical analysis, X-ray diffractometry, Raman spectroscopy and salt fog testing) were carried out in NaCl solution to evaluate the electrochemical hydrogen evolution efficiency and corrosion resistance of different electrodes/electrode supports, including Ni, Al, Ti, carbon cloth (CC), Cu and AISI 326L stainless steel [27]. Samples of Al and CC showed moderate and low corrosion at the applied potentials, indicating they are good catalyst supports. It is worth noting that Ni was the only sample which achieved the integration of high HER activity and electrocatalytic stability. Based on electrochemical impe-

dance spectroscopy, the Ni electrode presented a single process related to hydrogen generation, which is in contrast to the three processes (hydrogen generation, electrochemical corrosion and modification of organic groups on the surface of the electrode) of other samples in Cl^- -containing media. AISI 326L stainless steel with a high Ni content also showed high corrosion resistance, indicating Ni is a desirable electrode material in direct seawater electrolysis.

Except for high-concentration Cl^- , a further challenge for direct seawater electrolysis is fluctuations in pH values, as carbonate buffers are not sufficient to prevent localized changes in pH at both cathodes [28,29]. At the cathode of electrolyzer, an increase of pH during hydrogen evolution is inevitable, which can reach 5–9 pH units even the current density is lower than $10 \text{ mA} \cdot \text{cm}^{-2}$. Such a dramatic pH decrease near the cathode in the seawater without buffers may cause catalyst degradation and the precipitation of Mg^{2+} and Ca^{2+} , which are floccules and can block the electrode [30,31]. Actually, Mg^{2+} can make huge influence on the performance of the seawater electrolysis, especially long-term stability in seawater. The formation of surface and bulk precipitate during seawater electrolysis was investigated by varying current density and flow rate in 1982 [30]. Only in highly concentrated solutions the formation of surface precipitate can be reduced by increasing the current density. On the contrast, a high fluid flow rate is effective to reduce the formation of precipitate. The initial adhered precipitate formation take place at specific surface sites and the surface potential determines the growth rate. Even some recent reported HER electrocatalysts which can work in all-pH seawater electrolysis also show a high overpotential in unbuffered seawater [32,33]. More seriously, the decreased pH near the anode can lead to the activation of chloride chemistry as the chloride-related reactions become favorable at a relatively small pH value [34]. To ensure a high selectivity to OER and avoid ClER at the anode, the Pourbaix diagram states the smallest pH of 7.5, which cannot be realized in unartificial seawater electrolysis. Thus, until a better method is present, the addition of supporting buffers is indispensable for the stabilization of pH fluctuation.

Besides, other compositions in the seawater including non-innocent ions, microbial contaminations and solid impurities may also be toxic to the electrocatalysts at both electrodes, infecting their activities and long-term stabilities [21,35]. Therefore, the development of corrosion-resistant electrocatalysts with high selectivity and stability is the key to realize the large-scale application of direct seawater electrolysis.

3 Design of anode electrocatalysts for direct seawater electrolysis

Based on the above considerations of competing reactions and other challenges in direct seawater electrolysis, several

strategies are helpful for developing efficient anode electrocatalysts with OER-selectivity and long-term stability, including restricting chloride chemistry thermodynamically, manipulating the OER/ClER selectivity by OER-selective active species and using protective layers (Table 1).

3.1 Restricting chloride chemistry thermodynamically

The first strategy is to take advantage of the thermodynamic and kinetic differences between OER and ClER. It is considered that the anode electrocatalysts can work without the interference of chloride chemistry in specific applied voltage range where OER is thermodynamically allowed but ClER is thermodynamically restricted. Based on the Pourbaix diagram (Fig. 1(a)), this voltage range at different pH values can be summarized and the maximum allowed overpotentials for selective seawater electrolysis are shown in Fig. 2 [24]. When the pH-overpotential coordinate locates in the dashed area, an oxygen evolution selectivity of 100% can be obtained. Chlorine-related reactions are thermodynamically possible above the limiting lines, competing with kinetically unfavored OER. It is observed that there are alleviated conditions for 100% selective OER in alkaline conditions with an overpotential of about 480 mV, indicating that developing highly efficient electrocatalysts in an alkaline environment with overpotentials at lower than 480 mV at the desired current density can effectively prevent the interference of chloride chemistry.

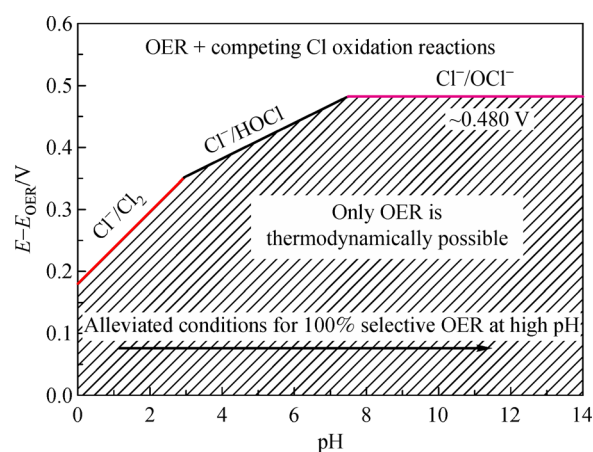


Fig. 2 Maximum allowed overpotential region where only OER is thermodynamically possible in seawater electrolysis. The $E - E_{\text{OER}}$ values are the difference between chloride-related reactions (chlorine evolution, hypochlorous acid formation and hypochlorite formation reaction) and OER at different pH values. Reprinted with permission from ref. [24], copyright 2016, Wiley-VCH.

Most of the early works on developing electrocatalysts for selective seawater electrolysis were based on this strategy. In 1990, Bennet [31] proposed that a high

Table 1 Oxygen evolution electrocatalysts reported in saline electrolyte

| Catalyst | Support | Electrolyte | Prominent performance | Ref. |
|---|----------------------|---|---|------|
| (MnMo)O _x | IrO ₂ /Ti | 0.5 mol·L ⁻¹ NaCl | OER selectivity of 91% | [36] |
| (Mn-W)O _x | IrO ₂ /Ti | 0.5 mol·L ⁻¹ NaCl | OER selectivity of 99.6% | [37] |
| Co ₃ O ₄ | Ni foam | 1 mol·L ⁻¹ KOH + natural seawater | Overpotential: about 280 mV for HER and 450 mV for OER at 100 mA·cm ⁻² | [38] |
| Co-Fe-O-B | Glassy carbon | 1 mol·L ⁻¹ KOH + 0.5 mol·L ⁻¹ NaCl | Overpotential: 294 mV for OER at 10 mA·cm ⁻² | [39] |
| (Mn _{0.88} Mo _{0.12})O _{2,12} | IrO ₂ /Ti | 0.5 mol·L ⁻¹ NaCl | OER selectivity of 99.6% after 1500 h electrolysis at 100 mA·cm ⁻² | [40] |
| NiFe-LDH | Membrane | 0.5 mol·L ⁻¹ KOH + 0.5 mol·L ⁻¹ NaCl | Stable electrolysis at 200 mA·cm ⁻² for 100 h | [41] |
| S-(Ni ₁ Fe)OOH | Ni foam | 1 mol·L ⁻¹ KOH + natural seawater | Overpotential of 300 and 398 mV for OER at 100 and 500 mA·cm ⁻² | [42] |
| NiCoS | Ni foam | 1 mol·L ⁻¹ KOH + natural seawater | Stable electrolysis at 800 mA·cm ⁻² | [43] |
| RuO ₂ /Zn | Ti mesh | 150 mmol·L ⁻¹ NaCl + 0.1 mol·L ⁻¹ HClO ₄ | Change of selectivity by the incorporation of Zn | [44] |
| Pb ₂ Ru ₂ O _{7-x} | Glassy carbon | 0.1 mol·L ⁻¹ NaOH + 0.6 mol·L ⁻¹ NaCl | OER selectivity of 99% at pH = 13 and 5 h stable electrolysis at 200 mA·cm ⁻² | [45] |
| Co-Se ₄ | Co foil | Buffered seawater (pH = 7.09) | 10.3 mA·cm ⁻² at 1.8 V for overall seawater electrolysis | [46] |
| Co-Pi | Glassy carbon | 0.5 mol·L ⁻¹ NaCl + 0.1 mol·L ⁻¹ Pi (pH = 7.0) | Retained activity for O ₂ generation in Cl ⁻ -containing electrolyte | [47] |
| Co/Co ₃ O ₄ @C | Carbon fiber paper | 1 mol·L ⁻¹ KOH + natural seawater | Overpotential: about 600 mV for HER and 630 mV for OER at 10 mA·cm ⁻² | [48] |
| Co-Fe LDH | Ti mesh | Simulated seawater (pH = 8.0) | Stable electrolysis for a diurnal cycle (8 h·d ⁻¹) | [49] |
| MnO _x /IrO _x | Glassy carbon | 30 mmol·L ⁻¹ KCl + 0.5 mol·L ⁻¹ KHSO ₄ | CER selectivity decreased from 86% to 7% by MnO _x deposition | [50] |
| CaFeO ₄ /FePO ₄ | FTO | Buffered synthetic seawater (pH = 7.0) | Overpotential: about 710 mV for OER at 10 mA·cm ⁻² and stable electrolysis for over 10 h | [51] |
| GO@Fe@Ni-Co | Ni foam | 1 mol·L ⁻¹ KOH + 0.5 mol·L ⁻¹ NaCl | 20 and 1000 mA·cm ⁻² at 1.57 and 2.02 V for overall seawater electrolysis | [52] |
| NM/IrO ₂ | Ti mesh | 0.5 mol·L ⁻¹ NaCl (pH = 8.3) | OER selectivity of nearly 100% by Nafion coating | [53] |
| NiFe/NiS _x | Ni foam | 1 mol·L ⁻¹ KOH + 0.5 mol·L ⁻¹ NaCl | Stable electrolysis at 1000 mA·cm ⁻² for over 500 h | [54] |

selectivity to OER can be obtained at a low current density below $1 \text{ mA} \cdot \text{cm}^{-2}$ in which the noticeable limitations of CIER mass-transfer favor OER. In most instances, the low current density region ($< 1 \text{ mA} \cdot \text{cm}^{-2}$) indicates the required overpotential is below the maximum permission, thus restricting the chloride-related reactions thermodynamically. Accordingly, in 1997, a series of oxide mixtures of Mn and Ir, Ru, Pt, Fe, Co, Ni, Sn, La, Ce or Mo supported on IrO_2 -coated Ti ($(\text{Mn-M})\text{O}_x/\text{IrO}_2/\text{Ti}$ electrode, M means the additives) were synthesized for highly selective oxygen evolution in seawater electrolysis [36]. With the addition of small amounts of Ni, Co, Fe and Sn, the oxygen evolution efficiency was obviously enhanced, reaching the maximum value of 91% for $(\text{MnMo})\text{O}_x/\text{IrO}_2/\text{Ti}$ at $20 \text{ mA} \cdot \text{cm}^{-2}$ in $0.5 \text{ mol} \cdot \text{L}^{-1}$ NaCl (pH = 8), higher than that of 68%–70% for $\text{MoO}_x/\text{IrO}_2/\text{Ti}$. However, the addition of noble metals (Ru, Pt and Ir) induced the degradation of oxygen evolution activity in chloride-containing electrolytes, reflecting the influence of different doping metal additives. Single orthorhombic nanocrystalline γ - MnO_2 -type phase manganese-tungsten oxides ($(\text{Mn-W})\text{O}_x$) with homogeneously distributed Mn^{4+} and W^{6+} were also reported [37], and the efficiency for oxygen evolution could be enhanced to 99% at $20 \text{ mA} \cdot \text{cm}^{-2}$ even at pH 0.5.

Some recent studies have also used relatively low current densities to improve oxygen evolution selectivity in seawater electrolysis [38,39], suitable for the seawater electrolyzer powered by photovoltaic electricity or wind power-based electricity. However, the seawater electrolysis at high current densities ($> 100 \text{ mA} \cdot \text{cm}^{-2}$) needs more active electrocatalysts to decrease overpotentials (lower than 480 mV) in alkaline conditions at the desired current densities. Since 1999, Hashimoto's group has designed a series of γ - MnO_2 -type phase oxide mixtures, including Mn-Mo, Mn-Mo-W, Mn-Mo-Fe and Mn-Mo-Sn, and tested their electrocatalysts at high current densities of 100 or $200 \text{ mA} \cdot \text{cm}^{-2}$ [40,55–60]. It is worth noting that the single γ - MnO_2 -type structure of different oxides improved the oxygen evolution efficiency and the long-term stability

in saline water electrolysis could be resolved by preventing the oxidation of the inner Ti substrate using IrO_x as a protective layer.

Till now, numerous highly efficient OER electrocatalysts which can deliver a high current density at low overpotentials ($< 480 \text{ mV}$) have been developed. Among them, transition-metal (oxy)hydroxides, especially the NiFe-based ones have been considered as the most efficient candidates for overall water electrolysis, exhibiting high electrochemical performances in Cl^- -containing solutions for direct seawater electrolysis. A nanostructured NiFe-layered double hydroxide (NiFe-LDH) catalyst was synthesized for the application in the alkaline electrolyzer selectively splitting artificial alkaline seawater [41]. The required overpotential for a high current density of $290 \text{ mA} \cdot \text{cm}^{-2}$ was under 480 mV, which basically met the demand of industrial medium size electrolyzers. The seawater electrolyzer electrodes which are assembled by NiFe-LDH and Pt nanoparticles worked in 100 h tests at a maximum current density of $200 \text{ mA} \cdot \text{cm}^{-2}$ at 1.6 V. The loss of initial activities could be attributed to the unsuitability of membrane rather than the degradation of catalyst. Similarly, an ultrafast room-temperature method to synthesize Ni foam supported S-doped Ni/Fe (oxy) hydroxide (S-(NiFe)OOH) layer with extraordinary OER performance in seawater splitting was developed (Fig. 3) [42]. The S-(NiFe)OOH required only 398 mV to reach the desired current density of $500 \text{ mA} \cdot \text{cm}^{-2}$ in alkaline natural seawater, as shown in Fig. 3(a), which was derived from its desirable hydrophilic features and hierarchical porosity. In overall alkaline seawater electrolysis, low voltages (1.837 and 1.951 V) were required for the commercial demanded current densities (500 and $1000 \text{ mA} \cdot \text{cm}^{-2}$) and kept constant for more than 100 h. Besides, Ni foam supported three-dimensional (3D) hetero-lateral $\text{Ni}_3\text{S}_2/\text{Co}_3\text{S}_4$ nanosheets (NiCoS) were developed for alkaline seawater electrolysis [43]. Superior resistance to chloride corrosion and abundant active sites were obtained in the in situ grown Ni/Co (oxy)hydroxide surface layer, reaching

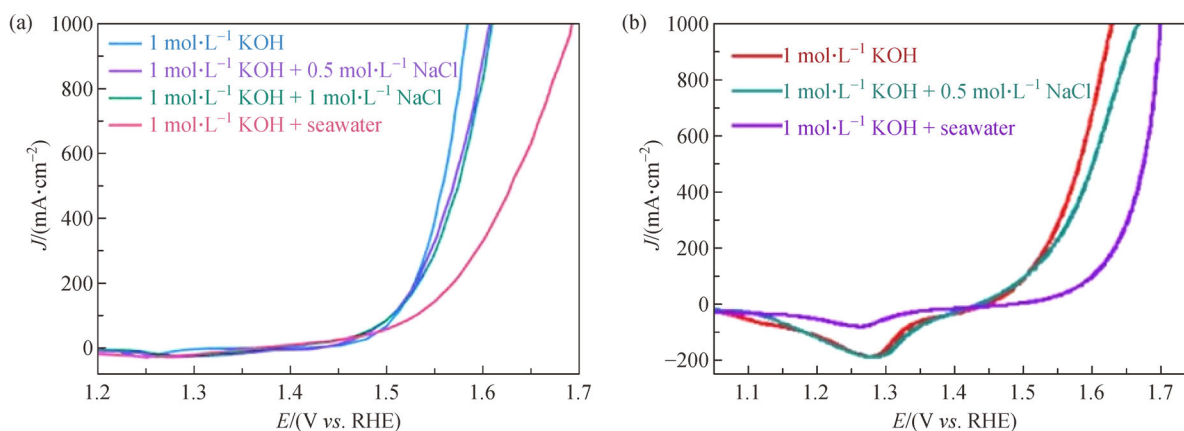


Fig. 3 Polarization curves for the (a) S-(NiFe)OOH and (b) NiCoS electrode tested in different electrolytes. Reprinted with permission from ref. [42], copyright 2020, Royal Society of Chemistry and ref. [43], copyright 2021, Elsevier, respectively.

$1 \text{ A}\cdot\text{cm}^{-2}$ at an overpotential of 0.47 mV in $1 \text{ mol}\cdot\text{L}^{-1}$ KOH + seawater (Fig. 3(b)). The NiCoS-catalyzed electrolyzer worked steadily at the industrial-level high current density of $800 \text{ mA}\cdot\text{cm}^{-2}$ for overall seawater splitting with no indication of chloride corrosion and could be integrated with photovoltaic system to reach an impressive solar-to- H_2 efficiency of 15.13%.

3.2 Active species selective to OER

For many electrocatalysts, it is difficult to achieve high current density at an overpotential of less than 480 mV. Another strategy for selective oxygen evolution in direct saline water electrolysis is to develop catalysts containing active species which are highly selective toward OER RI. This strategy is feasible regardless of pH but challenging since active species should be regulated and modified to separate closely related OER and chlorine chemistry [61]. Basically, it requires the modulation of existing active species or the development of new types of active sites.

Ru-based electrocatalysts have proved their advantageous physicochemical properties in overall pure water electrolysis, however, most of them show inferior performances and unsatisfying stability in direct saline water electrolysis due to the interference of Cl^- -related reactions. Some experimental investigations have focused on tailoring the selectivity of OER on Ru-based materials. The synthesis of Ru-Zn-O catalysts was first reported in 2010, in which the structure of RuO_2 active sites was tailored by Zn substitution (Fig. 4) [44]. In the vicinity of Zn ions, the Ru local atomic structure has been rearranged, which affects the chlorine evolution process by preventing the formation of rate-limiting intermediates of peroxo bridges. The X-ray absorption data supported the favorable modification of active sites and the Ru-Zn-O oxides show significant selectivity to oxygen evolution even in acidic NaCl-containing electrolyte (Fig. 4(a)), confirmed by the voltammetry results combined with different electrochemical mass spectroscopy. The construction of ruthenate pyrochlore structure of $\text{Pb}_2\text{Ru}_2\text{O}_{7-x}$ [45] has also been

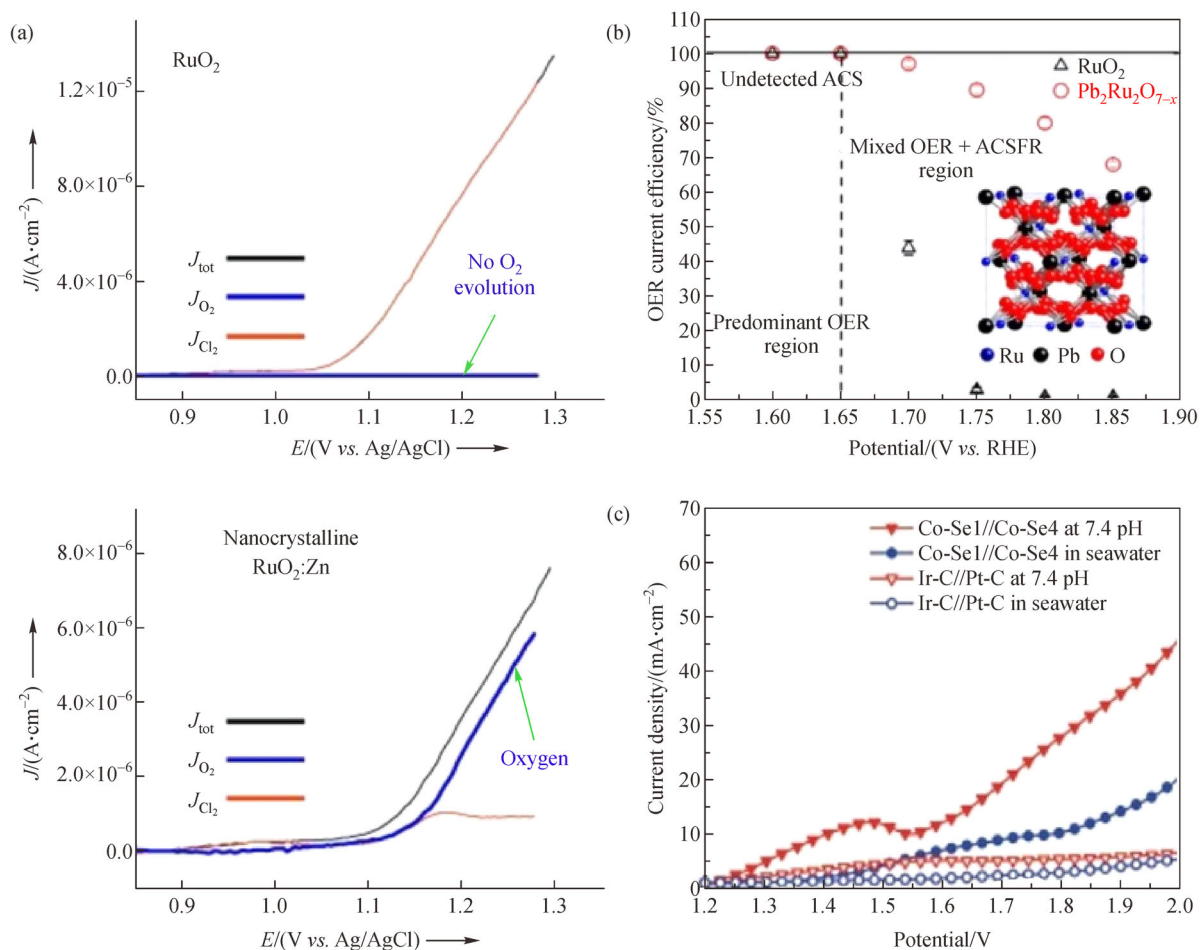


Fig. 4 (a) Original current density (black) and current densities attributed to oxygen (black) and chlorine (red) for anodic OER in $0.1 \text{ mol}\cdot\text{L}^{-1}$ $\text{HClO}_4 + 0.14 \text{ mol}\cdot\text{L}^{-1}$ NaCl solution. Reprinted with permission from ref. [44], copyright 2010, Wiley-VCH. (b) OER current efficiencies at various potentials for PbRu_2O_7 and RuO_2 in $0.6 \text{ mol}\cdot\text{L}^{-1}$ NaCl. Reprinted with permission from ref. [45], copyright 2020, American Chemical Society. (c) Polarization curves of Co-Se1//Co-Se4 and Ir-C//Pt-C in buffer solution and seawater. Reprinted from with permission ref. [46], copyright 2018, Wiley-VCH.

proved to enhance the oxygen evolution efficiency of Ru-based catalysts because of the higher concentration of oxygen vacancies and surface Ru(V) compared to RuO₂ (Fig. 4(b)). The Pb₂Ru₂O_{7-x} showed a high OER selectivity of about 99% at pH = 13 and worked at 200 mA·cm⁻² for over 5 h with only 10 mV voltage loss.

Many works have focused on Co-based catalysts which can be operated in neutral media and are considered as a promising catalyst for direct electrolysis in near-neutral seawater. By the selenization of Co foils, a 3D cobalt selenide containing CoSe and Co₉Se₈ was developed as a bifunctional electrocatalyst [46]. The charge state of Co species was modulated by controlling Co/Se mass ratio to enhance electrocatalytic performance since oxygen evolution activity and hydrogen evolution activity could be enhanced by the high charge state and the low charge state of Co, respectively. The resultant catalysts can be used in neutral phosphate buffered saline water with pH = 7.09 (Fig. 4(c)). Co-based phosphate/borate electrocatalysts like Co-Pi, Co-Bi and Co-MePi were developed through an electrolyte-dependent electrodeposition approach by Nocera's group [47]. Those catalysts could retain the catalytic activity of oxygen evolution in chloride-containing aqueous solutions. The proton-accepting characteristics of Co-Pi in phosphate electrolyte is responsible for the stable electrolysis at a high current density without chloride-related reactions. When mixed with carbon, a novel multifunctional Co/Co₃O₄@C can be synthesized by carbonizing the zeolite imidazolate framework and carbon fiber paper [48]. The Co/Co₃O₄-containing carbon material showed efficient HER and OER performances in the overall splitting in actual seawater. Co³⁺ species favored the oxidation of OH⁻ and electrophilic adsorption for the enhancement of oxygen evolution process. These samples highlights the importance of modulation of active species, tuning the key steps or RI of the OER or Cl⁻-related reactions. The substitution or dopants in the catalysts may change the charge state and regulate the adsorption energy of different RI, achieving relatively high selectivity to oxygen evolution. However, an in-depth understanding of the underlying mechanism origins of activities in these reports has not been clarified and further work is needed to explain the enhanced oxygen evolution selectivities through *in situ* electrochemical measurements and theoretical studies.

Though saline seawater usually leads to activity degradation of catalysts, several electrocatalysts show superior electrochemical performance in seawater electrolysis compared to that in pure water. For example, separate nucleation and aging steps were used to synthesize Co-Fe LDH which showed high oxygen reduction activity with an overpotential of 530 mV at 10 mA·cm⁻² and a high selectivity to OER in seawater (pH = 8), superior to those in pure water [49]. It was revealed by EDS and XPS analysis that Mg, Na, Cl and S elements existed on the surface of the Co-Fe LDH after the electrocatalysis-

process, which was due to the anion-exchange ability afforded by typical layered structure and high surface area. The comparative electrochemical measurements in simple electrolytes (NaCl, MgCl₂ and Na₂SO₄) demonstrated faster reaction kinetics, lower charge transfer resistance and better stabilities in seawater. The synergistic effect of various ions plays an important role in promoting electrocatalytic activity, in which the combined contribution of increased strong basic sites by Mg and Na ions, stabilized high valence states of Co by chloride ions and mediated proton transfers by F and Br ions resulted in the improved activity.

3.3 Protecting layers

Due to the complicated reaction mechanisms in natural seawater electrolysis, it is an efficient strategy to employ OER-selective or permselective protecting layers on the surface of electrocatalysts. Based on this strategy, the competing reactions of OER and ClER on manganese oxide (MnO_x) were investigated and MnO_x was employed as a permeable overlayer (Fig. 5) [50]. Glassy carbon-supported hydrous oxide (IrO_x/GC) was used as the active phase with electrodeposited MnO_x films (Fig. 5(a)). In the presence of Cl⁻ (30 mmol·L⁻¹), the ClER selectivity decreased from 86% to 7% upon the deposition of MnO_x onto IrO_x, proving that the MnO_x overlayer indeed prevented the interference of chloride-related reactions for higher OER selectivity. The MnO_x deposition could prevent the Cl⁻ transfer onto the surface of IrO_x catalyst but favor the transport of O₂, protons and water between the electrolyte and IrO_x for enhanced OER activity. Although the MnO_x film was considered as a catalytically inactive phase in this report, manganese oxides are widely known as efficient OER electrocatalysts. The protecting MnO_x layer may also act on unwanted ClER at a higher anodic potential, which need to be further verified. Similarly, FePO₄ can be electrodeposited onto CaFeO_x through spin-coating and subsequent annealing process [51]. The modification by electrodeposited CaFeO_x overlayer on the surface not only mitigated Mg²⁺-induced fouling, but also prevented the hypochlorite corrosion from chloride oxidation. The resultant CaFeO_x modified by FePO₄ only showed a moderate increase of about 70 mV in long-term stability test, which was attributed to the pH change in phosphate-buffered seawater solution (pH = 7). Besides, a CeO_x layer was deposited on highly active NiFeO_x electrocatalysts to achieve a highly stable performance [62]. The perm-selective CeO_x protecting layer was composed of mixed hydroxides and oxides, preventing the loss of OER-active Fe species and the diffusion of dissolved metal ion species, ferrocyanide, iodide and other redox ions between the catalyst and electrolyte while allowing the transport of O₂ and OH⁻ (Fig. 5(b)).

Some relatively inert materials seem also favorable to protect the activity of underlying catalysts from chloride

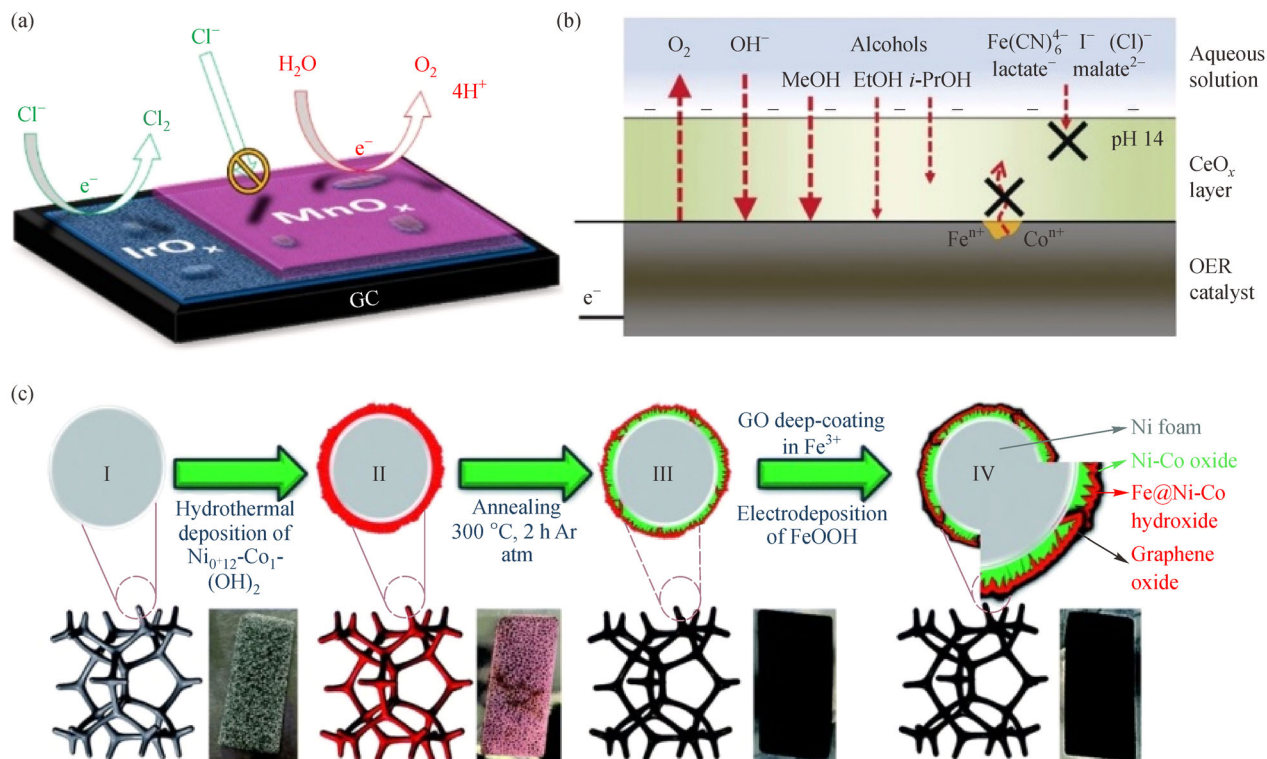


Fig. 5 (a) Sketch of OER and CIER on IrO_x/GC catalyst with and without MnO_x deposition. Reprinted with permission from ref. [50], copyright 2018, American Chemical Society. (b) Representation of the improved selectivity and stability on active NiFeO_x catalyst with CeO_x deposition. Reprinted with permission from ref. [62], copyright 2018, Wiley-VCH. (c) Schematic illustration of the preparation of GO@Fe@Ni-Co@NF. Reprinted with permission from ref. [52], copyright 2020, Royal Society of Chemistry.

corrosion and other challenges. An outer graphene oxide (GO) layer on FeOOH deposited β -Ni-Co hydroxide catalyst (GO@Fe@NiCo@NF) (Fig. 5(c)) was reported [52], which required a low overpotential of 345 mV for a high current density of 1 A·cm⁻² in alkaline seawater. The synergistic effect between the underneath metal oxide layer, Ni-Co hydroxide 2D sheets and interfacial FeOOH nanoparticles lowered the overpotentials for OER and the charge transfer resistance. In addition, the *in situ* generated oxidized carbon layer, GO overlayer and the lower interlayer distance of β -Ni-Co LDH synergistically prevented the chloride corrosion in direct seawater splitting, contributing to the stable performance in stability testing for up to 378 h. The selective enhancement for OER over CIER was also focused on [53], using cation-selective polymer Nafion as a perm-selective membrane surface-modifying IrO₂/Ti electrode for highly selective oxygen evolution at the anode of seawater electrolysis. Nearly 100% oxygen evolution efficiency could be obtained on Nafion solution coated/IrO₂/Ti in 0.5 mol·L⁻¹ NaCl electrolyte (pH = 8.3) since the Nafion membrane could electrostatically repel the transportation of chloride ions from electrolyte to the surface of IrO₂. Notably, the above protecting layers of GO overlayer and Nafion coating favor their inertness, which could work at industrial conditions with high current densities surviving from the interference

of competing reactions and other corruptions. Besides, these methods can be extended to other active oxygen evolution electrocatalysts for enhanced stability in direct seawater electrolysis with no conflict response. Nevertheless, these overlayers may to some degree limit H₂O or O₂ transportation, leading to inferior electrode performances. Further work should focus on preventing such negative effects when using these inert blocking overlayers.

Apart from overlayers on the surface of active species, a Ni foam supported NiS layer coated by Ni-Fe hydroxide (NiFe/NiS_x-Ni) catalyst was reported, in which the NiFe catalyst coating was responsible for high oxygen evolution activity drawing anodic currents toward water oxidation and the underneath sulfide layer led to *in situ* generated sulfate and carbonate cation-selective layers for repelling chloride [54]. With the superior corrosion resistance derived from this unique structure, the NiFe/NiS_x-Ni showed desirable catalytic performance in alkaline seawater electrolysis in terms of more than 1000 h at 1 A·cm⁻².

4 Design of cathode electrocatalysts for direct seawater electrolysis

Different from anode oxygen evolution electrocatalysts

which are subject to complex competitive reactions by chloride, the design of cathode hydrogen evolution electrocatalysts involves less attention to enhance the selectivity of electrode materials, since the thermodynamic potential gap between HER and its competing reactions is much lower than that between OER and Cl^- -related reactions. By contrast, the primary concerns for cathode electrocatalysts operating in natural seawater are related to undesirable cationic species and other impurities. Various dissolved ions in natural seawater may be reduced and electrodeposited on the surface of the electrode, leading to the degradation of active sites. Other impurities, including solid nanoparticles and microbial compositions, also pose a threat to the long-term stability of cathode electrocatalysts because they can be physical blockages on the surface of the electrode. Specific impurities that affect the performance of the cathode depend on the specific seawater environment. Thus, it is beneficial to develop efficient cathode electrocatalysts with resistance to the majority of undesirable impurities for highly stable water electrolysis performance in seawater.

The optimal metal-hydrogen binding energy (HBE) of Pt indicates its nearly best activity toward hydrogen evolution and Pt catalysts are currently the benchmark of hydrogen evolution electrocatalysts. However, in direct seawater electrolysis, the application of Pt catalysts is very challenging since the impurities in seawater may poison Pt

catalysts, leading to severe activity degradation. Thus, some Pt-based catalysts with the incorporation of other compositions or matrixes were reported. The corrosion-resistant Ni-Mo matrix anchored highly dispersed Pt nanoparticles was developed through a reduction-potential dependent sequential reduction process [63]. Compared with Pt/C catalyst, the high activity and durability in harsh conditions such as strong alkaline electrolyte and high temperature was attributed to the strongly anchored trace precious metal on a corrosion-resistant matrix with high surface area (Fig. 6). Pt-based alloys have also been developed with the addition of transition metals. Based on Brewer-Engel bond theory which illustrates the kinetically favorable hydrogen evolution mechanism on alloys with possible *d*-orbital overlapping, different Pt-based alloys were reported [64]. For example, a series of alloyed PtM (M = Mo, Ni, Co, Fe and Cr) supported on Ti mesh were fabricated [65]. The alloying effects by the incorporation of guest M species led to enhanced hydrogen evolution activities compared with pristine Pt electrodes, while the enhanced long-term durability in Cl^- -containing electrolyte was attributed to the competitive dissolution reaction between Pt and M with Cl_2 . The optimal PtMo alloy suffered only 9.87% of the initial current density loss after continuous operation in real seawater at about $150 \text{ mA} \cdot \text{cm}^{-2}$ for 172 h. Alloyed Pt-Ru-M (M = Mo, Ni, Co, Fe and Cr) was also prepared to confirm the promotion

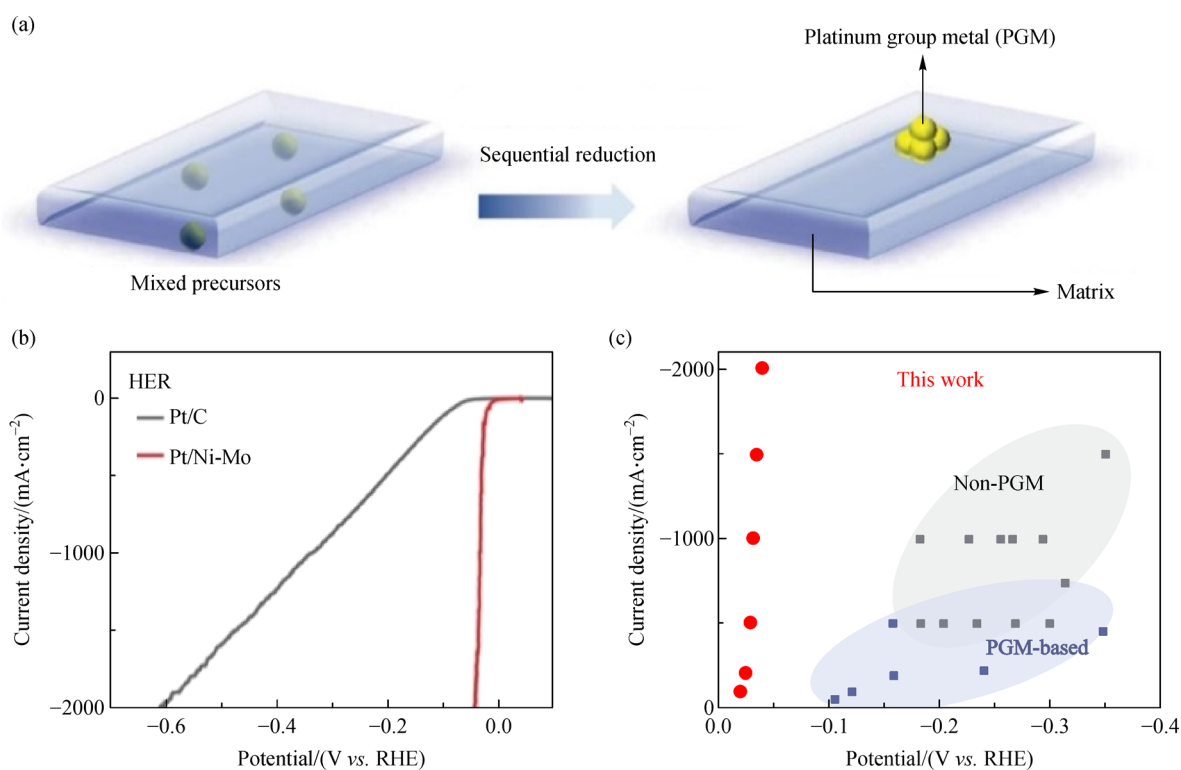


Fig. 6 (a) Reduction potential-dependent sequential reduction of platinum group metal (PGM) in Ni-Mo matrix; (b) hydrogen evolution polarization curves of Pt/C and Pt/Ni-Mo; (c) the comparison of the Pt/Ni-Mo and other PGM-based and Non-PGM catalysts. Reprinted with permission from ref. [63], copyright 2021, Wiley-VCH.

effect of alloying effects on electrocatalytic performance [66].

Though the high cost of Pt-based materials can be properly reduced by decreasing the content of Pt in alloys, the presence of Cl^- impurities in saline water can hinder the electrocatalytic activity of Pt-based electrodes and cause catalyst poisoning [67]. The efficient transition metal-based electrocatalysts with stable corrosion resistance in natural seawater are desirable as a substitute for low-cost and large-scale H_2 production. Ni-based electrocatalysts which act as a promising alternative to commercial Pt/C catalyst in pure water electrolysis have attracted interests in the application of direct seawater electrolysis. Because of the strong electron interaction between Ni and Mo atoms, the inclusion of Mo atoms in the nickel matrix enhances their intrinsic catalytic activity and reaction kinetics. Ni foam supported two hybrid NiMo films by electrodeposition in different electrolytes were synthesized [68], showing superior hydrogen evolution efficiency and corrosion resistance in seawater, which was attributed to the synergistic effect between Ni and Mo species. NiO was the main active species, facilitating the initial water dissociation and the following H_2 adsorption and desorption. Nanostructured Ni-Mo-S was grown on carbon fiber cloth as an efficient HER electrocatalyst in neutral electrolyte [69]. The superior catalytic activity to the Mo-S catalyst was derived from substantial defects and atomic-scale modified morphology by the incorporation of Ni atoms. The accumulation of generated H_2 bubbles could be prevented by the reduced aggregations in Ni-Mo-S/C, thus enhancing the long-term hydrogen evolution stability in seawater electrolysis. By thermal ammonolysis of NiMoO_4 precursor, a Cu foam supported NiMoN nanowire array modified by Ni nanoparticles was synthesized [70]. The

nanowire array imparted the underwater superhydrophobic electrode surface for the detachment of H_2 bubbles from electrodes, while the Ni nanoparticles facilitated the dissociation of absorbed water for proton supply. The Ni/NiMoN nanowire array thus exhibited exceptional hydrogen evolution electrocatalytic performance to realize a current density of $10 \text{ mA} \cdot \text{cm}^{-2}$ with a low overpotential of only 37 mV in neutral electrolyte.

When combined with Fe atoms, a Ni-Fe-C electrocatalyst was developed by electrodeposition at current densities from 10 to $30 \text{ mA} \cdot \text{cm}^{-2}$ [71]. The carbon content and grain size were proved to affect the hydrogen evolution overpotential and reaction current density of Ni-Fe-C. The resultant catalyst with optimal carbon content and grain size showed stable electrochemical properties in Cl^- -containing solution at 90°C . An anisotropic surface doping energy was proposed employing dopants of a metal oxide with high OH binding energy and a metal with high HBE on a weak HBE metal surface [72]. The water dissociation can be facilitated by the high HBE metal and the high OH binding energy metal oxide, while the weak HBE metal surface promotes hybrid coupling. Ni and CrO_x sites were doped on a Cu surface ($\text{CrO}_x/\text{Cu-Ni}$) by this strategy to synthesize an efficient multi-site electrocatalyst for hydrogen evolution in neutral media. Since the incorporation of N atoms in transition metal-based catalysts, especially constructing a N-enriched structure in metal nitrides can promote the corrosion resistance in seawater by increasing the valence state of metal species, a Ni-inducing growth method was reported to synthesize N-rich Mo_5N_6 nanosheets with atom-scale thickness (Fig. (7)), in which N was incorporated into the Mo lattice [73]. This method endowed the resultant material with abundant metal-N active sites and high valence state of Mo

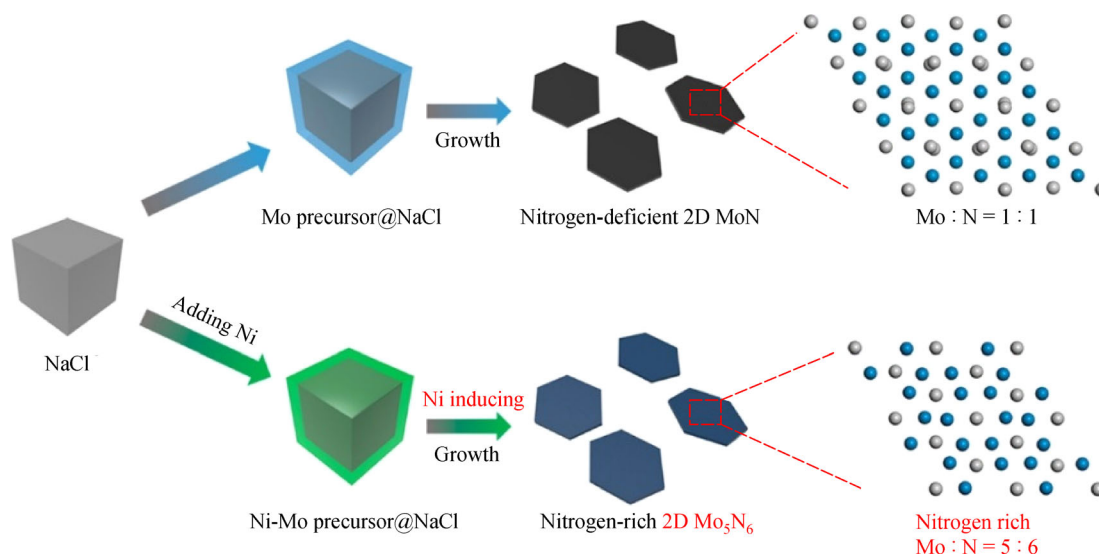


Fig. 7 Schematic illustration of the preparation of nitrogen-deficient 2D MoN and nitrogen 2D Mo_5N_6 electrocatalysts through an ammonization synthesis without and with Ni-induced process, respectively. Reprinted with permission from ref. [73], copyright 2018, American Chemical Society.

atoms as well as Pt-like electronic structure, all of which made the prepared single-crystal electrocatalyst highly efficient for HER in all pH electrolyte and natural seawater. Ni single atoms anchored porous N-doped carbon (Ni-SA/NC) was recently fabricated [74]. The threefold Ni atoms in Ni-N₃ coordination were responsible for the high hydrogen evolution electrocatalytic activity of the prepared catalyst, and abundant active sites were formed on the N-doped carbon by well-isolated Ni atoms. The Ni-SA/NC exhibited a low overpotential of 139 mV to realize a current density of 10 mA·cm⁻² and suffered negligible current attenuation after 14 h operation at 200 mA·cm⁻² in seawater. Nickel cobalt nitride and nickel phosphide microsheet arrays integrated catalyst with sandwich-like structure were also reported for efficient hydrogen evolution in seawater [75]. The high HER electrocatalytic activity and impressive stability in seawater was attributed to the high electrical conductivity, large surface area and outstanding Cl⁻ resistance of the inner Ni_xP microsheet array.

Similar to the design of anode oxygen evolution electrocatalysts, fabricating highly efficient cathode hydrogen evolution electrocatalysts with permselective protecting layers is another feasible strategy for stable operation in seawater electrolysis (Fig. 8) [76]. A layered N-doped carbon shell was used to coat cobalt molybdenum phosphide nanocrystal (CoMoP@C) (Fig. 8(a)) for substitute of Pt-based catalysts for hydrogen evolution in seawater [77]. The CoMoP@C catalyst exhibited superior HER activity in nearly all pH electrolytes and stable performances with a high Faradaic efficiency of 92.5% when operated in real seawater. The carbon shell not only provided strong proton absorption capacity to promote hydrogen evolution efficiency, but also protected the CoMoP core from poisoning in seawater. A urea-derived Co-encased N-doped carbon nanotubes (Fig. 8(b)) was

also synthesized [33], showing stable hydrogen evolution activity at all pH values and even in buffered seawater (pH = 7).

5 Design of bifunctional electrocatalyst for seawater electrolysis

For direct seawater electrolysis, the design of OER/HER bifunctional electrocatalysts is typically desired, as the materials developed can be fully utilized and the system of electrolytic equipment can easily be simplified without cross-contamination between anodes and cathodes [78–81]. Various non-precious bifunctional electrocatalysts have been developed for overall pure water electrolysis, including transition metal compounds, perovskites and carbon materials [82–86], while most of the reported materials are not available for direct seawater electrolysis due to the challenging environment in seawater. Typically, for the development of bifunctional electrocatalysts for direct seawater electrolysis, the corrosion resistance in Cl⁻-containing electrolyte can be improved by a hydrochloric acid-participating synthesis strategy, since the resultant electrocatalyst can maintain its structure stable in a harsh corrosion condition. Free-standing NiFe hydroxides were fabricated by corrosion engineering to be a high-performance bifunctional electrocatalyst for seawater electrolysis [87]. The strong interaction between metals and Cl ions favored the *in situ* formation of NiFe hydroxides by promoting the dissolution of Ni ions from NiFe foam. The HCl corrosion induced sample could be applied in a two-electrode system for operation in alkaline seawater for 300 h at 100 mA·cm⁻², showing its high chloride tolerance and outstanding stability. Similarly, a heterogeneous bimetallic phosphide Ni₂P-Fe₂P was synthesized as a bifunctional electrocatalyst for direct

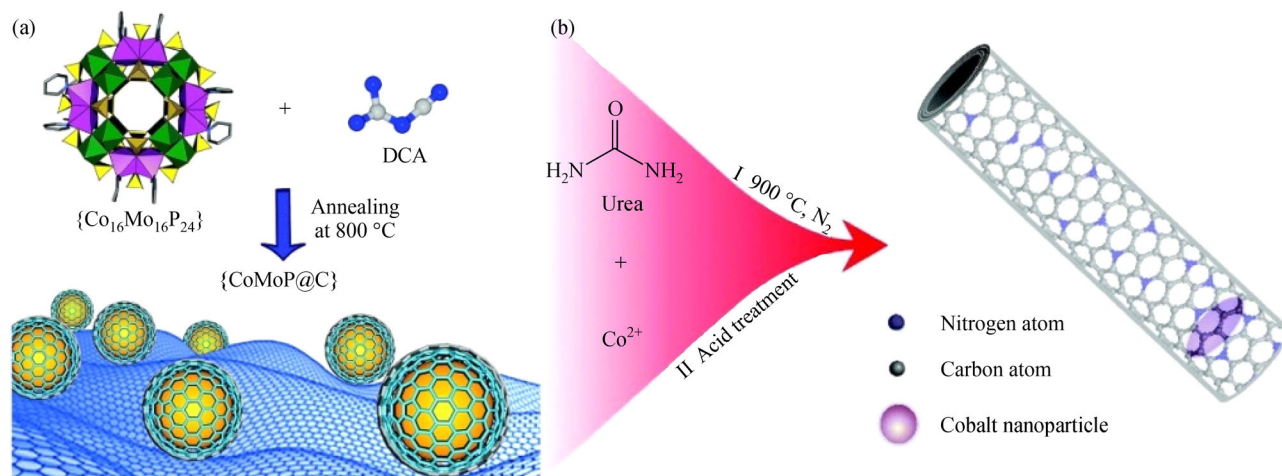


Fig. 8 Schematic illustration of the preparation of (a) CoMoP@C catalyst and (b) U-CNT-900 catalyst. Reprinted with permission from ref. [77], copyright 2017, Royal Society of Chemistry and ref. [33], copyright 2015, Royal Society of Chemistry.

water electrolysis by a two-step route, in which the Ni foam was soaked in a solution containing HCl and $\text{Fe}(\text{NO}_3)_3$, followed by a phosphorization treatment [88]. The hydrophilic surface and corrosion resistance to chloride ions favored its application in Cl^- -containing seawater.

In a vacuum-sealed ampoule, a Ni_3N and Ni_3S_2 -interfaced electrode electrocatalyst was synthesized [89], exhibiting excellent oxygen evolution and hydrogen evolution electrocatalytic performance in neutral electrolyte and seawater. The outstanding catalytic activity was attributed to abundant interfacial regions between Ni_3S_2 and Ni_3N active species, which could facilitate the adsorption and dissociation of water molecules. Recently, a trimetallic catalyst (Ni-Mo-Fe) supported by graphitic carbon felt has also been synthesized for alkaline seawater and natural seawater electrolysis [90], with an energy efficiency of up to 65% and stable electrocatalytic performance in seawater for over 24 h. The Ni-Mo-Fe electrocatalyst was reported to reconfigure into different structure under anodic and cathodic bias and the undesired deposition of CaCO_3 could be removed rapidly through a simple regeneration technique. The inert substrate and alkalized condition were responsible for the highly suppressed chloride chemistry [23,91,92].

6 Design of seawater electrolyzers

The implement of direct seawater electrolysis not only depends on the rational design of electrocatalysts on electrodes, but also requires highly efficient and stable electrolyzers. The design criteria of seawater electrolyzer mandate the anodic overpotential of < 480 mV and the total electrolyte pH of > 7.5 to prevent the interpretation of competing chlorine chemistry, which has been discussed in earlier sections [93]. Currently, prevalent water electrolysis technologies at low-temperature (< 100 °C) include anion exchange membrane water electrolyzers (AEMWE), proton exchange membrane water electrolyzers (PEMWE) and alkaline water electrolyzers (AWE) [94,95].

Commonly, an anion exchange membrane (AEM) is placed at the center of electrolyser and water feed is only supplied to the cathode, where H_2 and OH^- can be generated [47,94]. OH^- then migrates through the AEM toward the OER catalyst at the anode. The unwanted migration of anions like Cl^- cannot be limited by the AEM, indicating the competition between oxygen evolution and chlorine chemistry cannot be prevented even if feed water is not supplied to the anode. However, the oxidation of Cl^- can be minimized by the high operating pH in AEMWE for ease of direct seawater electrolysis. PEMWE holds similar configuration with AEMWE, except for that a solid acid polymer electrolyte as proton exchange membrane (PEM) is sandwiched between the two electrodes and water feed is commonly supplied to the anode [95–97]. Water is

oxidized at the anode to be O_2 and H^+ , and H^+ migrates through the solid electrolyte to the cathode where H_2 is produced. Anionic impurities can be isolated at the anode and cationic species like Mg^{2+} and Ca^{2+} can still migrate through the PEM to the cathodic area. AWE is separated by a porous diaphragm preventing gas crossover and both sides are filled with liquid alkaline electrolyte [97]. The porous diaphragm, compared to AEM and PEM, allows the migration of most cations and anions.

Due to the inescapable contact between Cl^- and anode as well as Mg^{2+} and cathode, similar problems exist on these three configurations, including unwanted competition with the formation of hypochlorite, blockages of precipitates and solid impurities on membranes and electrodes. Though some simple methods like periodical recovery procedures and filtration before the electrolysis can to some extent be effective, the development of novel configurations of seawater electrolysis is more desirable to achieve large-scale commercial application.

Asymmetric electrolyte feeding electrolyser was reported to increase the seawater electrolysis performance and avoid the undesired alkalization of electrolysis environment (Fig. 9) [98]. AEMWE with different feeding electrolytes in cathodic and anodic compartments were compared (Fig. 9(a)), and the asymmetric electrolyser using $0.5 \text{ mol} \cdot \text{L}^{-1}$ KOH solution in anodic compartment and natural seawater in cathodic compartment showed comparable performance to that of symmetric AEMWE using KOH electrolyte in both compartments, and superior performance to that of symmetric AEMWE using natural seawater in both compartments. In the asymmetric electrolyser, NiFe-LDH as the anodic OER electrocatalyst showed comparable performance to that of Ir-based benchmark catalysts with ultrahigh cell voltages of 4.0 V. The unique configuration made the NiFe-LDH highly selective to OER without any oxidation of Cl^- though trace amounts of Cl^- could migrate through the AEM to the anodic compartment, ensuring selective and stable seawater electrolysis. PEMWE using seawater vapor from ambient humidity at near-surface ocean conditions were also demonstrated to efficiently produce H_2 [99]. Air with 80% relative seawater-humidity and dry N_2 were used in the anode and cathode compartments, respectively. This solar-driven electrolyser can maintain a high electrolysis current density to achieve a solar-to- H_2 conversion efficiency of 6.3% after operating for 50 h, while only 0.5% for the liquid seawater feeding counterpart. The feasibility of this seawater-vapor electrolyser is the result of bypassing the liquid seawater-related catalyst fouling issues by impurities. GO can also be applied as the proton-conducting membrane in seawater-vapor electrolyser due to its good through-plane proton conductivity (Fig. 9(b)) [100]. The GO membrane fitted with anode of $\text{IrO}_2\text{-Al}_2\text{O}_3$ and cathode of Pt/C can efficiently produce H_2 from seawater-humidified air with good H_2 and O_2 evolution rates close to theoretical values.

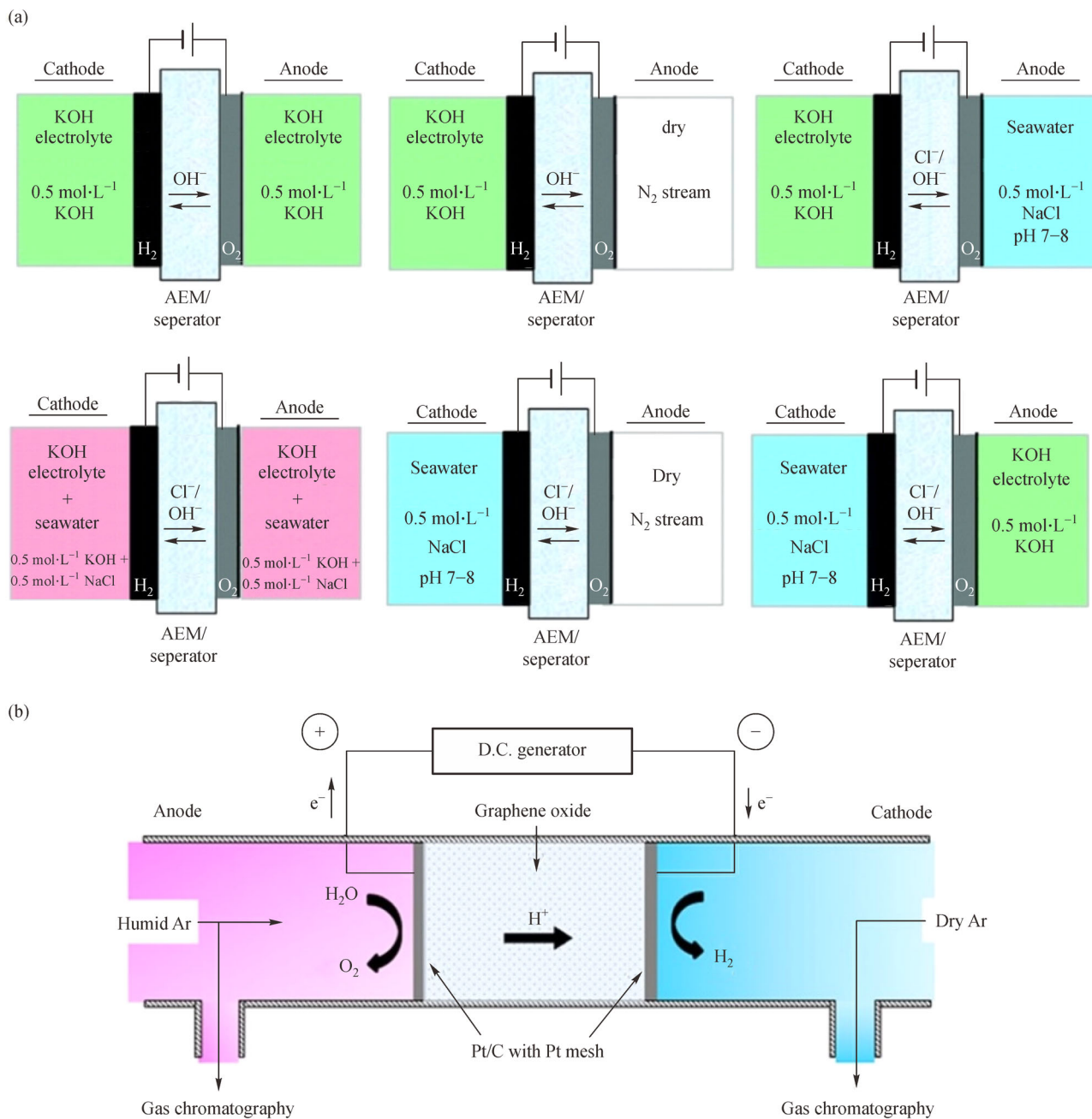


Fig. 9 (a) Schemes for AEMWE using asymmetric feeding electrolyte with different electrolyte composition. Reprinted with permission from ref. [98], copyright 2020, Royal Society of Chemistry. (b) Scheme of a GO device for concentration-cell measurements, hydrogen pumping and water vapor electrolysis. Reprinted with permission from ref. [100], copyright 2018, American Chemical Society.

7 Conclusions and future outlook

Seawater is considered an infinite resource, as it covers 97% of the earth, and fresh water seems to be increasingly precious today. To combat with global energy crisis and reduce the high cost for the incorporation of water purification systems into electrolyzers, direct electrolysis of natural seawater is an attractive but challenging method. The complicated composition of seawater, including

massive undesirable cations and anions, solid impurities and microbial contamination, leads to the interference of various competing reactions, blockage of the electrode surface and the degradation of electrode catalysts at both anode and cathode. Thus, direct seawater electrolysis requires rational design of electrode catalysts. At the anode, to limit the competing Cl^- -related reactions and promote the selectivity to oxygen evolution, “alkaline design criterion” is proposed. Applying suitable reaction

environment to control the overpotential below the thermodynamic equilibrium potential of chlorine chemistry can efficiently restrict Cl^- -related reactions. Besides, the design of OER-selective active species and employing permselective protecting layers have been proved to be effective strategies to favor oxygen evolution and prevent side-reactions and catalyst poisoning. At the cathode, the research mainly focus on the protection of undesirable cationic species and other impurities and many efficient and stable electrocatalysts were developed.

Even though many works have focused on the rational design of electrocatalysts for direct seawater electrolysis, several issues should be solved or noticed. 1) Though the main side-reactions of Cl^- -related reactions have been extensively studied, there is still a lack of understanding of the competition mechanisms between OER and CIER in specific active species, as well as other competitive reactions in natural seawater. The future experimental and calculation studies should address this issue. 2) The current research on direct seawater electrolysis requires a standardized test condition. Because the composition of seawater varies around the globe, the experimental results in different works are difficult to compare. Notably, the standardized electrolyte composition should be close to natural seawater near coastal arid regions, which is ideally suited for seawater electrolysis. Standard criteria is also needed for the parameters of long-term stability tests, in which a standard time and a current density should be stipulated. 3) Long-term stability remains a problem for many designed electrocatalysts. Employing perm-selective protecting layers or developing other efficient methods to enhance the durability of electrocatalysts in seawater is proposed. 4) Advanced characterization techniques, such as *in situ* microscopy and *in situ* X-ray spectroscopy should be used to detect the material reconstruction of anodic electrocatalysts during seawater electrolysis for further understanding of structure-stability-activity relationship. 5) Despite the development of active and stable electrocatalysts, creative design of electrolyser and corresponding application of proper membrane are also encouraging for efficient seawater electrolysis. This review discussed the design of anode and cathode electrocatalysts for direct seawater electrolysis based on the fundamental composition and possibly existed competing reactions in natural seawater, hopefully being helpful for promising progress in the future. Despite challenges, it is believed that the great efforts on theoretical calculation and experiment exploration will boost the construction of high-efficient electrocatalysts and promote the development of direct seawater electrolysis.

Acknowledgements This work was supported by the National Natural Science Foundation of China (Grant Nos. 22111530112 and 21875118), the Natural Science Foundation of Tianjin (Grant No. 19JCZDJC37700), and the Foundation of State Key Laboratory of High-efficiency Utilization of Coal and Green Chemical Engineering (Grant No. 2020-KF-22).

References

- Xu K, Cheng H, Lv H F, Wang J Y, Liu L Q, Liu S, Wu X J, Chu W S, Wu C Z, Xie Y. Controllable surface reorganization engineering on cobalt phosphide nanowire arrays for efficient alkaline hydrogen evolution reaction. *Advanced Materials*, 2018, 30(1): 1703322
- Liu T, Li P, Yao N, Cheng G Z, Chen S L, Luo W, Yin Y D. CoP-doped MOF-based electrocatalyst for pH-universal hydrogen evolution reaction. *Angewandte Chemie International Edition*, 2019, 58(14): 4679–4684
- Ren J T, Wang Y S, Chen L, Gao L J, Tian W W, Yuan Z Y. Binary FeNi phosphides dispersed on N,P-doped carbon nanosheets for highly efficient overall water splitting and rechargeable Zn-air batteries. *Chemical Engineering Journal*, 2020, 389: 124408
- Martindale B C M, Reisner E. Bi-functional iron-only electrodes for efficient water splitting with enhanced stability through *in situ* electrochemical regeneration. *Advanced Energy Materials*, 2016, 6(6): 1502095
- Zhang J W, Lv X W, Ren T Z, Wang Z, Bandosz T J, Yuan Z Y. Engineering heterostructured Ni@Ni(OH)₂ core-shell nanomaterials for synergistically enhanced water electrolysis. *Green Energy & Environment*, 2021, doi: 10.1016/j.gee.2020.12.009
- Ren J T, Chen L, Yang D D, Yuan Z Y. Molybdenum-based nanoparticles (Mo₂C, MoP and MoS₂) coupled heteroatoms-doped carbon nanosheets for efficient hydrogen evolution reaction. *Applied Catalysis B: Environmental*, 2020, 263: 118352
- Zheng Y, Jiao Y, Vasileff A, Qiao S Z. The hydrogen evolution reaction in alkaline solution: from theory, single crystal models, to practical electrocatalysts. *Angewandte Chemie International Edition*, 2018, 57(26): 7568–7579
- Ren J T, Yao Y, Yuan Z Y. Fabrication strategies of porous precious-metal-free bifunctional electrocatalysts for overall water splitting: recent advances. *Green Energy & Environment*, 2021, 6(5): 620–643
- Roger I, Shipman M A, Symes M D. Earth-abundant catalysts for electrochemical and photoelectrochemical water splitting. *Nature Reviews Chemistry*, 2017, 1: 0003
- Lv X W, Hu Z P, Chen L, Ren J T, Liu Y P, Yuan Z Y. Organic-inorganic metal phosphonate-derived nitrogen-doped core-shell Ni₂P nanoparticles supported on Ni foam for efficient hydrogen evolution reaction at all pH values. *ACS Sustainable Chemistry & Engineering*, 2019, 7(15): 12770–12778
- Zhang J W, Zhang H, Ren T Z, Yuan Z Y, Bandosz T J. FeNi doped porous carbon as an efficient catalyst for oxygen evolution reaction. *Frontiers of Chemical Science and Engineering*, 2021, 15(2): 279–287
- Ji X X, Lin Y H, Zeng J, Ren Z H, Lin Z J, Mu Y B, Qiu Y J, Yu J. Graphene/MoS₂/FeCoNi(OH)_x and graphene/MoS₂/FeCoNiP_x multilayer-stacked vertical nanosheets on carbon fibers for highly efficient overall water splitting. *Nature Communications*, 2021, 12(1): 1380
- Wang J, Kim S J, Liu J P, Gao Y, Choi S B, Han J W, Shin H Y, Jo S G, Kim J W, Ciucci F, et al. Redirecting dynamic surface restructuring of a layered transition metal oxide catalyst for

- superior water oxidation. *Nature Catalysis*, 2021, 4(3): 212–222
14. Ursua A, Gandia L M, Sanchis P. Hydrogen production from water electrolysis: current status and future trends. *Proceedings of the IEEE*, 2012, 100(2): 410–426
 15. Zhao H, Yuan Z Y. Design strategies of transition-metal phosphate and phosphonate electrocatalysts for energy-related reactions. *ChemSusChem*, 2021, 14(1): 130–149
 16. Turner J A. Sustainable hydrogen production. *Science*, 2004, 305(5686): 972–974
 17. Weng C C, Ren J T, Yuan Z Y. Transition metal phosphide-based materials for efficient electrochemical hydrogen evolution: a critical review. *ChemSusChem*, 2020, 13(13): 3357–3375
 18. Ren J T, Song Y J, Yuan Z Y. Facile synthesis of molybdenum carbide nanoparticles *in situ* decorated on nitrogen-doped porous carbons for hydrogen evolution reaction. *Journal of Energy Chemistry*, 2019, 32: 78–84
 19. Cuartero M, Crespo G, Cherubini T, Pankratova N, Confalonieri F, Massa F, Tercier-Waeber M L, Abdou M, Schäfer J, Bakker E. *In situ* detection of macronutrients and chloride in seawater by submersible electrochemical sensors. *Analytical Chemistry*, 2018, 90(7): 4702–4710
 20. Xiang C, Papadantonakis K M, Lewis N S. Principles and implementations of electrolysis systems for water splitting. *Materials Horizons*, 2016, 3(3): 169–173
 21. Tong W, Forster M, Dionigi F, Dresch S, Sadeghi Erami R, Strasser P, Cowan A J, Farràs P. Electrolysis of low-grade and saline surface water. *Nature Energy*, 2020, 5(5): 367–377
 22. Kester D R, Duedall I W, Connors D N, Pytkowicz R M. Preparation of artificial seawater. *Limnology and Oceanography*, 1967, 12(1): 176–179
 23. Yu L, Zhu Q, Song S, McElhenny B, Wang D, Wu C, Qin Z, Bao J, Yu Y, Chen S, Ren Z. Non-noble metal-nitride based electrocatalysts for high-performance alkaline seawater electrolysis. *Nature Communications*, 2019, 10(1): 5106
 24. Dionigi F, Reier T, Pawolek Z, Gliech M, Strasser P. Design criteria, operating conditions, and nickel-iron hydroxide catalyst materials for selective seawater electrolysis. *ChemSusChem*, 2016, 9(9): 962–972
 25. Exner K S, Sohrabnejad-Eskan I, Over H. A universal approach to determine the free energy diagram of an electrocatalytic reaction. *ACS Catalysis*, 2018, 8(3): 1864–1879
 26. Exner K S, Anton J, Jacob T, Over H. Controlling selectivity in the chlorine evolution reaction over RuO₂-based catalysts. *Angewandte Chemie International Edition*, 2014, 53(41): 11032–11035
 27. Ysea N, Diaz L A, Lacconi G I, Franceschini E A. Stability study of materials for electrode supports for the hydrogen generation from a NaCl aqueous solution. *Electrocatalysis*, 2021, 12(5): 537–547
 28. Auinger M, Katsounaros I, Meier J C, Klemm S O, Biedermann P U, Topalov A A, Rohwerder M, Mayrhofer K J J. Near-surface ion distribution and buffer effects during electrochemical reactions. *Physical Chemistry Chemical Physics*, 2011, 13(36): 16384–16394
 29. Katsounaros I, Meier J C, Klemm S O, Topalov A A, Biedermann P U, Auinger M, Mayrhofer K J J. The effective surface pH during reactions at the solid-liquid interface. *Electrochemistry Communications*, 2011, 13(6): 634–637
 30. Kirk D W, Ledas A E. Precipitate formation during sea water electrolysis. *International Journal of Hydrogen Energy*, 1982, 7(12): 925–932
 31. Bennett J E. Electrodes for generation of hydrogen and oxygen from seawater. *International Journal of Hydrogen Energy*, 1980, 5(4): 401–408
 32. Wu X, Zhou S, Wang Z, Liu J, Pei W, Yang P, Zhao J, Qiu J. Engineering multifunctional collaborative catalytic interface enabling efficient hydrogen evolution in all pH range and seawater. *Advanced Energy Materials*, 2019, 9(34): 1901333
 33. Gao S, Li G D, Liu Y, Chen H, Feng L L, Wang Y, Yang M, Wang D, Wang S, Zou X. Electrocatalytic H₂ production from seawater over Co, N-codoped nanocarbons. *Nanoscale*, 2015, 7(6): 2306–2316
 34. Karlsson R K B, Cornell A. Selectivity between oxygen and chlorine evolution in the chlor-alkali and chlorate processes. *Chemical Reviews*, 2016, 116(5): 2982–3028
 35. Oh B S, Oh S G, Hwang Y Y, Yu H W, Kang J W, Kim I S. Formation of hazardous inorganic by-products during electrolysis of seawater as a disinfection process for desalination. *Science of the Total Environment*, 2010, 408(23): 5958–5965
 36. Izumiya K, Akiyama E, Habazaki H, Kumagai N, Kawashima A, Hashimoto K. Effects of additional elements on electrocatalytic properties of thermally decomposed manganese oxide electrodes for oxygen evolution from seawater. *Materials Transactions*, 1997, 38(10): 899–905
 37. Izumiya K, Akiyama E, Habazaki H, Kumagai N, Kawashima A, Hashimoto K. Anodically deposited manganese oxide and manganese-tungsten oxide electrodes for oxygen evolution from seawater. *Electrochimica Acta*, 1998, 43(21): 3303–3312
 38. Niu J, Yang J, Channa A I, Ashalley E, Yang J, Jiang J, Li H, Ji H, Niu X. Enhancing the water splitting performance via decorating Co₃O₄ nanoarrays with ruthenium doping and phosphorization. *RSC Advances*, 2020, 10(45): 27235–27241
 39. Gupta S, Forster M, Yadav A, Cowan A J, Patel N, Patel M. Highly efficient and selective metal oxy-boride electrocatalysts for oxygen evolution from alkali and saline solutions. *ACS Applied Energy Materials*, 2020, 3(8): 7619–7628
 40. Fujimura K, Matsui T, Habazaki H, Kawashima A, Kumagai N, Hashimoto K. The durability of manganese-molybdenum oxide anodes for oxygen evolution in seawater electrolysis. *Electrochimica Acta*, 2000, 45(14): 2297–2303
 41. Dresch S, Dionigi F, Loos S, Ferreira de Araujo J, Spöri C, Gliech M, Dau H, Strasser P. Direct electrolytic splitting of seawater: activity, selectivity, degradation, and recovery studied from the molecular catalyst structure to the electrolyzer cell level. *Advanced Energy Materials*, 2018, 8(22): 1800338
 42. Yu L, Wu L B, McElhenny B, Song S W, Luo D, Zhang F H, Yu Y, Chen S, Ren Z F. Ultrafast room-temperature synthesis of porous S-doped Ni/Fe (oxy)hydroxide electrodes for oxygen evolution catalysis in seawater splitting. *Energy & Environmental Science*, 2020, 13(10): 3439–3446
 43. Wang C Z, Zhu M Z, Cao Z Y, Zhu P, Cao Y Q, Xu X Y, Xu C X, Yin Z Y. Heterogeneous bimetallic sulfides based seawater electrolysis towards stable industrial-level large current density.

- Applied Catalysis B: Environmental, 2021, 291: 120071
44. Petrykin V, Macounova K, Shlyakhtin O A, Krtil P. Tailoring the selectivity for electrocatalytic oxygen evolution on ruthenium oxides by zinc substitution. *Angewandte Chemie International Edition*, 2010, 49(28): 4813–4815
 45. Gayen P, Saha S, Ramani V. Selective seawater splitting using pyrochlore electrocatalyst. *ACS Applied Energy Materials*, 2020, 3(4): 3978–3983
 46. Zhao Y, Jin B, Zheng Y, Jin H, Jiao Y, Qiao S Z. Charge state manipulation of cobalt selenide catalyst for overall seawater electrolysis. *Advanced Energy Materials*, 2018, 8(29): 1801926
 47. Surendranath Y, Dincă M, Nocera D G. Electrolyte-dependent electrosynthesis and activity of cobalt-based water oxidation catalysts. *Journal of the American Chemical Society*, 2009, 131(7): 2615–2620
 48. Zhang Q J, Zhao X J, Miao X J, Yang W T, Wang C T, Pan Q H. ZIF-L-Co@carbon fiber paper composite derived Co/Co₃O₄@C electrocatalyst for ORR in alkali/acidic media and overall seawater splitting. *International Journal of Hydrogen Energy*, 2020, 45(58): 33028–33036
 49. Cheng F F, Feng X L, Chen X, Lin W G, Rong J F, Yang W S. Synergistic action of Co-Fe layered double hydroxide electrocatalyst and multiple ions of sea salt for efficient seawater oxidation at near-neutral pH. *Electrochimica Acta*, 2017, 251: 336–343
 50. Vos J G, Wezendonk T A, Jeremiasse A W, Koper M T M. MnO_x/IrO_x as selective oxygen evolution electrocatalyst in acidic chloride solution. *Journal of the American Chemical Society*, 2018, 140(32): 10270–10281
 51. Huang W H, Lin C Y. Iron phosphate modified calcium iron oxide as an efficient and robust catalyst in electrocatalyzing oxygen evolution from seawater. *Faraday Discussions*, 2019, 215: 205–215
 52. Jadhav A R, Kumar A, Lee J J, Yang T H, Na S Y, Lee J S, Luo Y G, Liu X H, Hwang Y, Liu Y, Lee H. Stable complete seawater electrolysis by using interfacial chloride ion blocking layer on catalyst surface. *Journal of Materials Chemistry. A, Materials for Energy and Sustainability*, 2020, 8(46): 24501–24514
 53. Balaji R, Kannan B S, Lakshmi J, Senthil N, Vasudevan S, Sozhan G, Shukla A K, Ravichandran S. An alternative approach to selective sea water oxidation for hydrogen production. *Electrochemistry Communications*, 2009, 11(8): 1700–1702
 54. Kuang Y, Kenney M J, Meng Y, Hung W H, Liu Y, Huang J E, Prasanna R, Li P, Li Y, Wang L, et al. Solar-driven, highly sustained splitting of seawater into hydrogen and oxygen fuels. *Proceedings of the National Academy of Sciences of the United States of America*, 2019, 116(14): 6624–6629
 55. Fujimura K, Matsui T, Izumiya K, Kumagai N, Akiyama E, Habazaki H, Kawashima A, Asami K, Hashimoto K. Oxygen evolution on manganese-molybdenum oxide anodes in seawater electrolysis. *Materials Science and Engineering A*, 1999, 267(2): 254–259
 56. Abdel Ghany N A, Kumagai N, Meguro S, Asami K, Hashimoto K. Oxygen evolution anodes composed of anodically deposited Mn-Mo-Fe oxides for seawater electrolysis. *Electrochimica Acta*, 2002, 48(1): 21–28
 57. El-Moneim A A, Kumagai N, Asami K, Hashimoto K. Nanocrystalline manganese-molybdenum-tungsten oxide anodes for oxygen evolution in acidic seawater electrolysis. *Materials Transactions*, 2005, 46(2): 309–316
 58. El-Moneim A A, Kumagai N, Hashimoto K. Mn-Mo-W oxide anodes for oxygen evolution in seawater electrolysis for hydrogen production. *Materials Transactions*, 2009, 50(8): 1969–1977
 59. Kato Z, Bhattarai J, Kumagai N, Izumiya K, Hashimoto K. Durability enhancement and degradation of oxygen evolution anodes in seawater electrolysis for hydrogen production. *Applied Surface Science*, 2011, 257(19): 8230–8236
 60. Kato Z, Sato M, Sasaki Y, Izumiya K, Kumagai N, Hashimoto K. Electrochemical characterization of degradation of oxygen evolution anode for seawater electrolysis. *Electrochimica Acta*, 2014, 116: 152–157
 61. Trasatti S. Electrocatalysis in the anodic evolution of oxygen and chlorine. *Electrochimica Acta*, 1984, 29(11): 1503–1512
 62. Obata K, Takanabe K. A permselective CeO_x coating to improve the stability of oxygen evolution electrocatalysts. *Angewandte Chemie International Edition*, 2018, 57(6): 1616–1620
 63. Yang F, Luo Y, Yu Q, Zhang Z, Zhang S, Liu Z, Ren W, Cheng H M, Li J, Liu B. A durable and efficient electrocatalyst for saline water splitting with current density exceeding 2000 mA·cm⁻². *Advanced Functional Materials*, 2021, 31(21): 2010367
 64. Jakšić M M. Electrocatalysis of hydrogen evolution in the light of the Brewer-Engel theory for bonding in metals and intermetallic phases. *Electrochimica Acta*, 1984, 29(11): 1539–1550
 65. Zheng J J, Zhao Y Y, Xi H, Li C H. Seawater splitting for hydrogen evolution by robust electrocatalysts from secondary M (M = Cr, Fe, Co, Ni, Mo) incorporated Pt. *RSC Advances*, 2018, 8(17): 9423–9429
 66. Li H Y, Tang Q W, He B L, Yang P Z. Robust electrocatalysts from an alloyed Pt-Ru-M (M = Cr, Fe, Co, Ni, Mo)-decorated Ti mesh for hydrogen evolution by seawater splitting. *Journal of Materials Chemistry. A, Materials for Energy and Sustainability*, 2016, 4(17): 6513–6520
 67. Camões M F, Anes B, Oliveira C S, Jorge M E M. Surface changes at platinumized platinum based hydrogen gas electrodes following use in highly saline aqueous solutions. *Electroanalysis*, 2014, 26(9): 1952–1957
 68. Yuan W, Cui Z, Zhu S, Li Z, Wu S, Liang Y. Structure engineering of electrodeposited NiMo films for highly efficient and durable seawater splitting. *Electrochimica Acta*, 2021, 365: 137366
 69. Miao J W, Xiao F X, Yang H B, Khoo S Y, Chen J Z, Fan Z X, Hsu Y Y, Chen H M, Zhang H, Liu B. Hierarchical Ni-Mo-S nanosheets on carbon fiber cloth: a flexible electrode for efficient hydrogen generation in neutral electrolyte. *Science Advances*, 2015, 1(7): e1500259
 70. Shang L, Zhao Y, Kong X Y, Shi R, Waterhouse G I N, Wen L, Zhang T. Underwater superaerophobic Ni nanoparticle-decorated nickel-molybdenum nitride nanowire arrays for hydrogen evolution in neutral media. *Nano Energy*, 2020, 78: 105375
 71. Song L J, Meng H M. Effect of carbon content on Ni-Fe-C electrodes for hydrogen evolution reaction in seawater. *International Journal of Hydrogen Energy*, 2010, 35(19): 10060–10066
 72. Dinh C T, Jain A, de Arquer F P G, De Luna P, Li J, Wang N,

- Zheng X, Cai J, Gregory B Z, Voznyy O, et al. Multi-site electrocatalysts for hydrogen evolution in neutral media by destabilization of water molecules. *Nature Energy*, 2019, 4(2): 107–114
73. Jin H, Liu X, Vasileff A, Jiao Y, Zhao Y, Zheng Y, Qiao S Z. Single-crystal nitrogen-rich two-dimensional Mo_5N_6 nanosheets for efficient and stable seawater splitting. *ACS Nano*, 2018, 12(12): 12761–12769
74. Zang W, Sun T, Yang T, Xi S, Waqar M, Kou Z, Lyu Z, Feng Y P, Wang J, Pennycook S J. Efficient hydrogen evolution of oxidized Ni-N₃ defective sites for alkaline freshwater and seawater electrolysis. *Advanced Materials*, 2021, 33(8): 2003846
75. Yu L, Wu L B, Song S W, McElhenny B, Zhang F H, Chen S, Ren Z F. Hydrogen generation from seawater electrolysis over a sandwich-like NiCoN[Ni₃P]/NiCoN microsheet array catalyst. *ACS Energy Letters*, 2020, 5(8): 2681–2689
76. Endrödi B, Sandin S, Smulders V, Simic N, Wildlock M, Mul G, Mei B T, Cornell A. Towards sustainable chlorate production: the effect of permanganate addition on current efficiency. *Journal of Cleaner Production*, 2018, 182: 529–537
77. Ma Y Y, Wu C X, Feng X J, Tan H Q, Yan L K, Liu Y, Kang Z H, Wang E B, Li Y G. Highly efficient hydrogen evolution from seawater by a low-cost and stable CoMoP@C electrocatalyst superior to Pt/C. *Energy & Environmental Science*, 2017, 10(3): 788–798
78. Gao X, Zhang H, Li Q, Yu X, Hong Z, Zhang X, Liang C, Lin Z. Hierarchical NiCo₂O₄ hollow microcuboids as bifunctional electrocatalysts for overall water-splitting. *Angewandte Chemie International Edition*, 2016, 55(21): 6290–6294
79. Ren J T, Yuan Z Y. Hierarchical nickel sulfide nanosheets directly grown on Ni foam: a stable and efficient electrocatalyst for water reduction and oxidation in alkaline medium. *ACS Sustainable Chemistry & Engineering*, 2017, 5(8): 7203–7210
80. Lv X W, Hu Z P, Ren J T, Liu Y P, Wang Z, Yuan Z Y. Self-supported Al-doped cobalt phosphide nanosheets grown on three-dimensional Ni foam for highly efficient water reduction and oxidation. *Inorganic Chemistry Frontiers*, 2019, 6(1): 74–81
81. Zhu Y P, Liu Y P, Ren T Z, Yuan Z Y. Self-supported cobalt phosphide mesoporous nanorod arrays: a flexible and bifunctional electrode for highly active electrocatalytic water reduction and oxidation. *Advanced Functional Materials*, 2015, 25(47): 7337–7347
82. Ling T, Yan D Y, Wang H, Jiao Y, Hu Z, Zheng Y, Zheng L, Mao J, Liu H, Du X W, Jaroniec M, Qiao S Z. Activating cobalt(II) oxide nanorods for efficient electrocatalysis by strain engineering. *Nature Communications*, 2017, 8(1): 1509
83. Song F Z, Li W, Yang J Q, Han G Q, Liao P L, Sun Y J. Interfacing nickel nitride and nickel boosts both electrocatalytic hydrogen evolution and oxidation reactions. *Nature Communications*, 2018, 9(1): 4531
84. Han N N, Yang K R, Lu Z Y, Li Y J, Xu W W, Gao T F, Cai Z, Zhang Y, Batista V S, Liu W, et al. Nitrogen-doped tungsten carbide nanoarray as an efficient bifunctional electrocatalyst for water splitting in acid. *Nature Communications*, 2018, 9(1): 924
85. Fabbri E, Nachtegaal M, Binninger T, Cheng X, Kim B J, Durst J, Bozza F, Graule T, Schäublin R, Wiles L, et al. Dynamic surface self-reconstruction is the key of highly active perovskite nano-electrocatalysts for water splitting. *Nature Materials*, 2017, 16(9): 925–931
86. Lv X W, Tian W W, Liu Y P, Yuan Z Y. Well-defined CoP/Ni₂P nanohybrids encapsulated in a nitrogen-doped carbon matrix as advanced multifunctional electrocatalysts for efficient overall water splitting and zinc-air batteries. *Materials Chemistry Frontiers*, 2019, 3(11): 2428–2436
87. Duan S, Liu Z, Zhuo H H, Wang T Y, Liu J Y, Wang L, Liang J S, Han J T, Huang Y H, Li Q. Hydrochloric acid corrosion induced bifunctional free-standing NiFe hydroxide nanosheets towards high-performance alkaline seawater splitting. *Nanoscale*, 2020, 12(42): 21743–21749
88. Wu L B, Yu L, Zhang F H, McElhenny B, Luo D, Karim A, Chen S, Ren Z F. Heterogeneous bimetallic phosphide Ni₂P-Fe₂P as an efficient bifunctional catalyst for water/seawater splitting. *Advanced Functional Materials*, 2021, 31(1): 2006484
89. Zhao Y Q, Jin B, Vasileff A, Jiao Y, Qiao S Z. Interfacial nickel nitride/sulfide as a bifunctional electrode for highly efficient overall water/seawater electrolysis. *Journal of Materials Chemistry. A, Materials for Energy and Sustainability*, 2019, 7(14): 8117–8121
90. Ros C, Murcia-López S, Garcia X, Rosado M, Arbiol J, Llorca J, Morante J R. Facing seawater splitting challenges by regeneration with Ni-Mo-Fe OER/HER bifunctional electrocatalyst. *ChemSusChem*, 2021, 14(14): 2872–2881
91. Xu S S, Lv X W, Zhao Y M, Ren T Z, Yuan Z Y. Engineering morphologies of cobalt oxide/phosphate-carbon nanohybrids for high-efficiency electrochemical water oxidation and reduction. *Journal of Energy Chemistry*, 2021, 52: 139–146
92. Zhao H, Yuan Z Y. Surface/interface engineering of high-efficiency noble metal-free electrocatalysts for energy-related electrochemical reactions. *Journal of Energy Chemistry*, 2021, 54: 89–104
93. Hsu S H, Miao J, Zhang L, Gao J, Wang H, Tao H, Hung S F, Vasileff A, Qiao S Z, Liu B. An earth-abundant catalyst-based seawater photoelectrolysis system with 17.9% solar-to-hydrogen efficiency. *Advanced Materials*, 2018, 30(18): 1707261
94. Vincent I, Bessarabov D. Low cost hydrogen production by anion exchange membrane electrolysis: a review. *Renewable & Sustainable Energy Reviews*, 2018, 81: 1690–1704
95. Carmo M, Fritz D L, Mergel J, Stolten D. A comprehensive review on PEM water electrolysis. *International Journal of Hydrogen Energy*, 2013, 38(12): 4901–4934
96. Chae K J, Choi M, Ajayi F F, Park W, Chang I S, Kim I S. Mass transport through a proton exchange membrane (Nafion) in microbial fuel cells. *Energy & Fuels*, 2008, 22(1): 169–176
97. Müller M, Carmo M, Glüsen A, Hehemann M, Saba S, Zwaygardt W, Stolten D. Water management in membrane electrolysis and options for advanced plants. *International Journal of Hydrogen Energy*, 2019, 44(21): 10147–10155
98. Dresch S, Ngo Thanh T, Klingenhof M, Brückner S, Hauke P, Strasser P. Efficient direct seawater electrolyzers using selective alkaline NiFe-LDH as OER catalyst in asymmetric electrolyte

- feeds. *Energy & Environmental Science*, 2020, 13(6): 1725–1729
99. Kumari S, Turner White R, Kumar B, Spurgeon J M. Solar hydrogen production from seawater vapor electrolysis. *Energy & Environmental Science*, 2016, 9(5): 1725–1733
100. Kida T, Kuwaki Y, Miyamoto A, Hamidah N L, Hatakeyama K, Quitain A T, Sasaki M, Urakawa A. Water vapor electrolysis with proton-conducting graphene oxide nanosheets. *ACS Sustainable Chemistry & Engineering*, 2018, 6(9): 11753–11758